Insights into Subtype Selectivity of Aurora Kinase Ligands from Molecular Dynamics Simulation

A Thesis Presented to

The Faculty of Graduate Studies Of

Lakehead University

By

Qianqian Wang

In partial fulfillment of requirements for the degree of

Master of Science

May 2024

ABSTRACT

Aurora kinases are phosphotransferase enzymes that play essential roles in cell division. There are three members of Aurora kinases in mammalian cells: Aurora A, Aurora B and Aurora C. The overexpression of Aurora kinases in diverse cancer cells make them promising targets in cancer therapy. Aurora kinases show highly conserved homology, having four different residues in the active site: Leu215, Thr217, Val218, and Arg220 in Aurora A (Arg159, Glu161, Leu162 and Lys164 in Aurora B). Therefore, understanding Aurora kinase inhibitor selectivity remains a top priority for kinase inhibitor design.

The utilization of molecular dynamics simulations for kinase selectivity studies could provide insights into ligand-protein interactions, including key residues, predominant free energy contributions, and interaction types, facilitating the design of subtype-selective inhibitors. To elucidate the subtype selectivity mechanism of Aurora kinase A and B, molecular docking was employed to construct complex structures. Subsequent MD simulations were conducted for complexes of Aurora A and B with selective inhibitors LY3295668, MK-5108, and Alisertib, as well as Aurora B selective inhibitor GSK-1070916 and pan-inhibitor Danusertib. The analysis included RMSD, average structure determination, MM/PBSA-derived binding free energy, and decomposition analysis, elucidating favorable or unfavorable residue contributions within the active site. For Aurora A selective inhibitors (LY3295668, MK-5108, and Alisertib), the residue Thr217 and Arg220/137 emerged as crucial for selectivity, with the carboxylate group being the predominant functional group contributing significantly to binding free energy in these compounds. Conversely, GSK-1070916's selectivity for Aurora B was attributed to Arg159 and Asp218, with its tertiary amine with methyl group being key functional groups. These findings on subtype selectivity mechanisms hold promise for the development of highly selective Aurora kinase inhibitors, offering a less toxic anti-cancer strategy.

Keywords

Aurora kinase, Aurora kinase inhibitor, Molecular dynamics simulation, LY3295668, MK-5108, Alisertib, GSK-1070916, Danusertib, subtype selectivity

Acknowledgments

Firstly, I would like to express my utmost gratitude to my supervisor, Dr. Jinqiang Hou, for his unwavering support and guidance throughout my academic journey. Dr. Hou has consistently demonstrated exceptional professionalism and responsibility, providing invaluable assistance in overcoming various academic challenges. During a period of physical and psychological difficulties that necessitated a temporary break from work, Dr. Hou's care and support were instrumental in my recovery and successful completion of the thesis. His encouragement played a pivotal role in helping me overcome psychological dilemmas and regain my health.

Secondly, I extend sincere appreciation to Dr. Michael Campbell and Dr. Wely Floriano for their valuable contributions as my committee members. Their courses significantly enriched my knowledge base, offering practical insights that greatly contributed to the development of this thesis. Special acknowledgment goes to Dr. Robert Mawhinney and Dr. Christine Gottardo for their understanding and support, especially when I faced health issues and needed to take a leave of absence from campus.

Furthermore, heartfelt thanks are due to the members of Dr. Hou's group, Dong Zhao, Yang Mao, and Wenjie Liu, who deserve special recognition for their unwavering support throughout this journey. Dong, in particular, provided valuable insights as she had done molecular dynamics simulation before me. I am grateful for our extensive discussions on research matters, and her patient assistance in addressing queries was truly invaluable. Dong and Yang not only contributed

significantly to my work but also provided care and support during times of illness and psychological challenges. My sincerest and special thanks go to them.

Lastly, I acknowledge and appreciate the support received from the Shared Hierarchical Academic Research Computing Network (SHARCNET, www.sharcnet.ca) for the generous allocation of computer resources.

TABLE OF CONTENTS

PAGE

CHAPTER ONE

Introduction

1.1 Cancer and Aurora Kinases

Cancer, a general term encompassing many diseases, can affect any part of body. A defining characteristic of cancer is the rapid production of abnormal cells that exceed their usual boundaries, invading neighbouring areas and leading to metastasis. In this process, cancer spreads to other organs. Extensive metastasis stands as the primary cause of cancer-related deaths[1]. Metastasis typically occurs in the late stages of cancer and can involve the blood or, lymphatic system, or both. The typical steps in metastasis include local invasion, entry into the bloodstream or lymphatic system, circulation throughout the body, extravasation into new tissues, proliferation, and angiogenesis[2,3]. Different types of cancer tend to metastasize to specific organs, with the lungs, liver, brain, and bones being the most common sites[4]. In Canada, cancer is the leading cause of death, accounting for 28.2% of all deaths (Fig. 1.1). In 2022, an average of 641 Canadians would be diagnosed with cancer every day, leading to 233 deaths daily[5].

A kinase is an enzyme that facilitates the transfer of phosphate groups from high-energy, phosphate-donating molecules to specific substrates[6]. As serine/threonine kinases and phosphotransferase enzymes, Aurora kinases play an essential role in cell proliferation[7]. There are three family members of Aurora kinases in Mammalian cells: Aurora A, Aurora B, and Aurora C, each possessing active and inactive modes. Aurora A functions during the prophase of mitosis, playing a crucial role in the formation of the mitotic spindle, centrosome separation, and the organization

and alignment of chromosomes. Aurora B, acting as a chromosome passenger protein, is involved in attaching the mitotic spindle to the centromere and chromosome segregation. Aurora C exclusively functions in germ-line cells during meiosis[8].

The overexpression of Aurora kinases in diverse cancer cells make them promising targets in cancer therapy[9]. Different kinds of cancer have different levels of survival correlation with Aurora kinases.

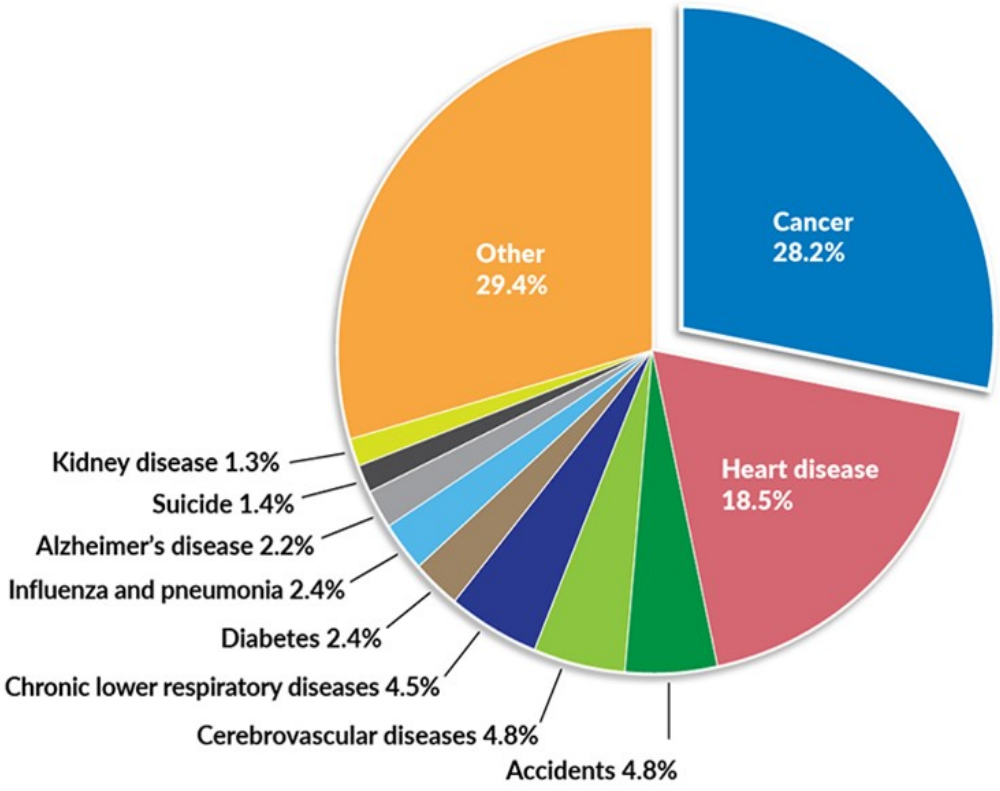

Fig. 1.1 Proportion of Deaths Due to Cancer and Other Causes, Canada, 2019

1.2 Aurora Kinase A, B and C

1.2.1 Aurora Kinase A

Aurora kinase A, encoded by the AURKA gene in humans, is implicated in crucial processes during both mitosis and meiosis, essential for healthy cell proliferation[10]. Aurora A is activated through one or more phosphorylation events, with its activity peaking during the G2 phase to M phase transition in the cell cycle[11].

Aurora kinases were initially identified in 1990 during a cDNA screen of Xenopus eggs, and the significance of Aurora A in meiosis and mitosis was recognized in 1998[12]. Aurora A localizes near the centrosome during late G1 phase and early S phase, associating with mitotic poles and adjacent spindle microtubules as the cell cycle progresses[13,14]. Aurora A remains associated with the spindles through telophase and relocalizes to the mid-zone of the spindle just before mitotic exit[15].

During mitosis, Aurora A is critical for proper mitotic spindle formation, separation of centrosomes, and organization and alignment of chromosomes during prometaphase[16]. Additionally, it contributes to completing cytokinesis, ensuring the cell's exit from mitosis[17,18]. Dysregulation of Aurora A has been associated with a high occurrence of cancer, as its proper expression is crucial for preventing aneuploidy[19-21].

1.2.2 Aurora Kinase B

In the past decade, numerous studies have associated aberrant expression of Aurora kinases with cancer, leading to the development of Aurora kinase inhibitors[22]. Aurora B is crucial for

chromosome segregation, spindle points, and cytoplasmic division, and alterations in these processes can induce aneuploidy, a key characteristic of cancer cells[23].

Aurora kinase B functions in attaching the mitotic spindle to the centromere and forms complexes with three other proteins: Survivin, Borealin, and INCENP[24]. Each component is essential for the proper localization and function of the others. Aurora B, a chromosomal passenger protein, reaches its expression peak at the G2-M transition, with maximum activity during mitosis[25]. It localizes to chromosomes in prophase, centromeres in prometaphase and metaphase, and the central mitotic spindle in anaphase[26,27].

Abnormally elevated levels of Aurora B kinase result in unequal chromosomal separation during cell division, causing cells to possess abnormal chromosome numbers[28,29]. Aurora B acts both as a cause and driver of cancer[30]. Inhibiting Aurora B kinase allows polyploid cells to continue dividing, but severe chromosomal abnormalities may eventually halt division or lead to cell death[31-33]. Aurora B is involved in chromosomal bi-orientation, spindle assembly checkpoint control, and cytokinesis regulation, and its overexpression is observed in various cancers[34-36].

1.2.3 Aurora Kinase C

Aurora kinase C, encoded by the AURKC gene in humans, is an enzyme that localizes to centrosomes during early mitosis, and subsequently translocates to the midzone of mitotic cells from anaphase to cytokinesis[37,38]. Its expression in diploid human fibroblasts is approximately one order lower than that of Aurora Kinase B, with mRNA and protein concentrations peaking during

the G2/M phase[39]. Notably, the peak expression of Aurora kinase C in the M phase occurs later than that of Aurora kinase B[40]. While Aurora Kinase A and B are primarily expressed in mitotic somatic cells, Aurora Kinase C is predominantly expressed in spermatogenesis and oogenesis during meiosis. Although its expression is typically limited to meiotic cells, overexpression has been observed in certain cancer cell lines[41].

1.3 Structures of Aurora Kinases

Aurora A consists of a short N-terminal domain and a highly evolutionarily conserved C-terminal catalytic domain (Fig. 1.2), similar to Aurora B and C. The N-terminal domain marks the start of a protein or polypeptide, while the C-terminal domain marks the end. The N-terminal domain comprises a five-stranded antiparallel β sheet, an essential regulatory αC helix, and a P-loop[42]. The αC helix, a unique and dynamically regulated element within the protein kinase molecule, belongs to the N-lobe in terms of sequence. The P-loop, a phosphate-binding loop, typically consists of a glycine-rich sequence followed by a conserved lysine and a serine or threonine[43]. The C-terminal domain is predominantly α helical and contains the activation loop (A-loop), which is involved in polypeptide substrate binding[44]. The activation loop is typically 20 to 30 residues in length and starts with a conserved DFG motif (usually Asp-Phe-Gly)[45]. The directionality of the three residues of the DFG motif in the activation loop differs between active and inactive Aurora Kinases[46]. In active proteins, the activation loop extends away from the binding site, while in inactive proteins, it is folded towards the binding site. Additionally, Aurora A's partner protein is TPX2, whereas

Aurora B's partner protein is INCENP[47].

In active kinase structures, this loop forms a cleft that binds the substrate. These two domains are connected by a flexible joint called the kinase hinge region, with the ATP binding pocket located between them. The ATP binding site is the active site in Aurora Kinases[48].

Aurora kinase exhibits a wide range of conformations between active and inactive states. The active conformation features several structural characteristics. In this state, the activation loop moves away from the hinge region and the ATP pocket, facilitating the binding of substrate peptides[49]. The DFG motif points into the ATP-binding pocket, adopting a DFG-in conformation, with its side chains facing the αC helix in opposite orientations. Moreover, in this state, the αC helix is relatively close to the ATP binding pocket, with the conserved glutamic acid on the αC helix pointing toward the ATP binding pocket[50]. Residues downstream of the DFG motif in the activation loop typically form a short α-helix, and a residue (tyrosine, serine, or threonine) in the activation loop is phosphorylated[51].

In the inactive conformation, the activation loop adopts a closed conformation, blocking substrate binding. The DFG motif points away from the ATP binding pocket, adopting a DFG-out conformation, with the conserved glutamic acid on the α-C helix facing the solvent-exposed region[52]. Crystal structures of several kinases in the inactive state indicate that the activation loop adopts a range of conformations, all of which are in a closed state, with residues of the activation loop remaining unphosphorylated[53].

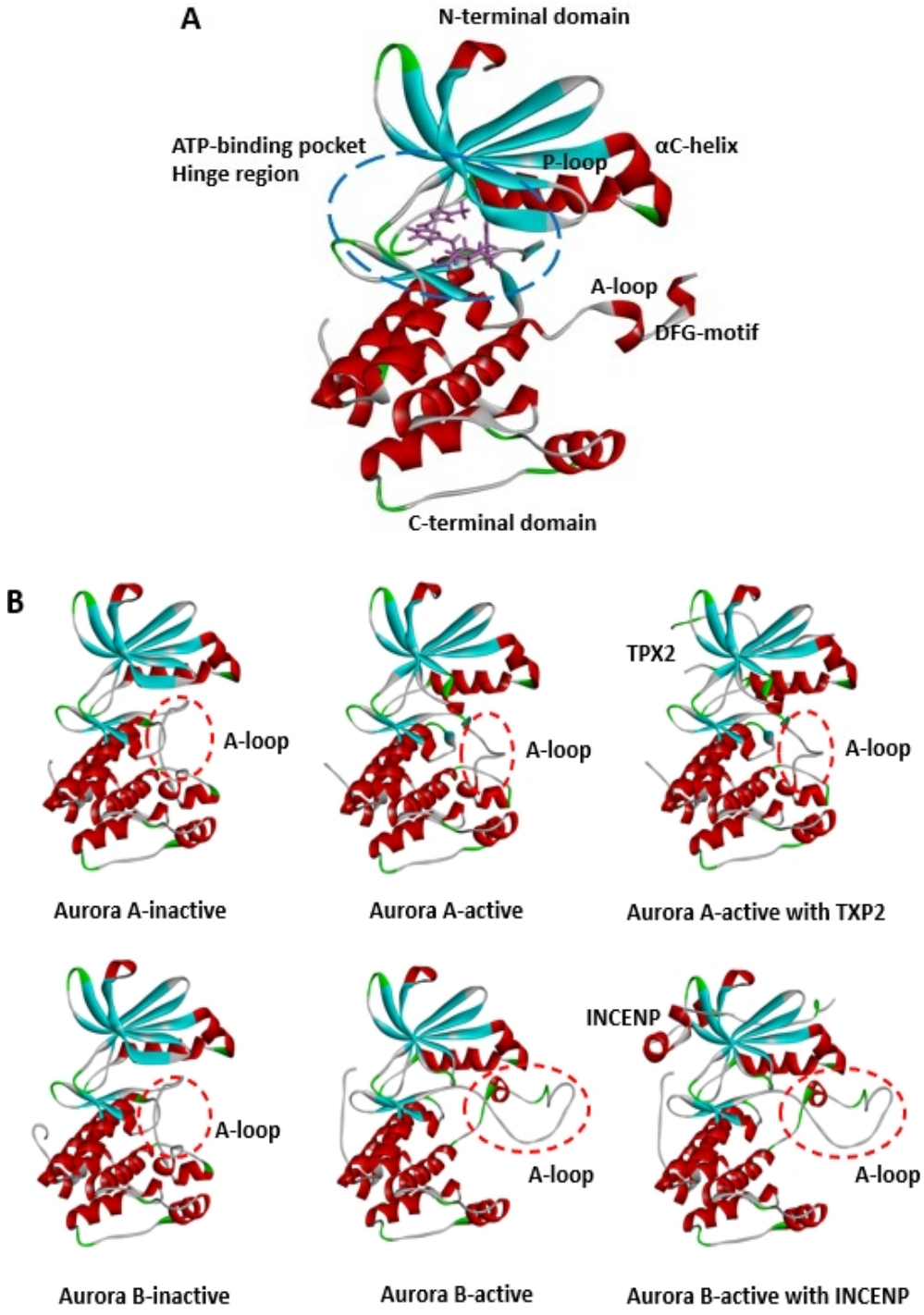

Fig. 1.2 (A) Crystal structure of Aurora A-active with LY3295668 (6C2R). (B) Different directions of DFG motif in activation loop in active and inactive Aurora Kinases.

1.4 High homology of Aurora Kinases

Aurora kinases exhibit highly conserved homology, differing only in four residues within the active site: Leu215, Thr217, Val218, and Arg220 in Aurora A (Arg159, Glu161, Leu162, and Lys164 in Aurora B)[54] (Fig. 1.3)[55]. Aurora kinases share a common catalytic core, resulting in significant sequence and structural similarity. Aurora kinase A and B, B and C, A and C demonstrate a notable degree of identity at the primary sequence level. The kinase domain is highly conserved among Aurora proteins, with homologies of 71%, 60%, and 75% between Aurora A and Aurora B, Aurora A and Aurora C, Aurora B and Aurora C, respectively (Fig. 1.4)[56]. These sequence and structural similarities may contribute to a lack of selectivity and off-target toxicity of kinase inhibitors. Therefore, understanding Aurora kinase inhibitor selectivity remains a top priority for kinase inhibitor design and clinical safety assessment.

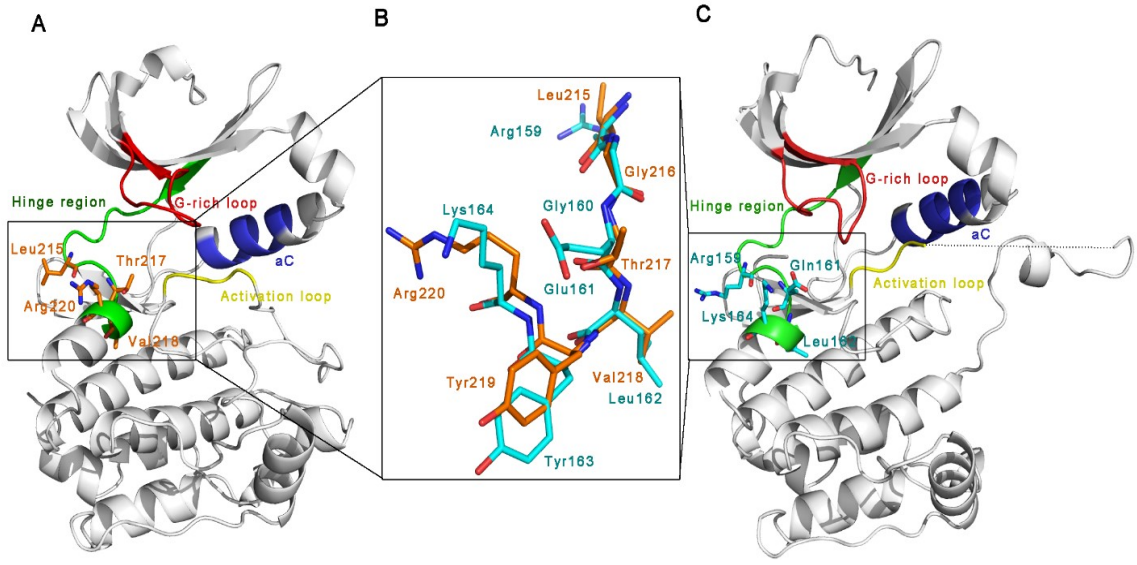

Fig. 1.3 (A) The crystal structure of human Aurora kinase A (PDB ID: 3E5A). Illustration of the structural segments of the ATP-binding pocket: the hinge region and the first two residues of the

αD helix (green), the Gly-rich loop (red), the residues in the αC helix (blue) and the ADFG residues in the activation loop (yellow). (B) Superposition of the hinge residues of Aurora A and B shows that only four residues in the hinge region and αD helix differ in human Aurora A and B. They are colored in orange and cyan in Aurora A and B, respectively. (C) The crystal structure of human Aurora kinase B (PDB id: 4AF3)[55,57]

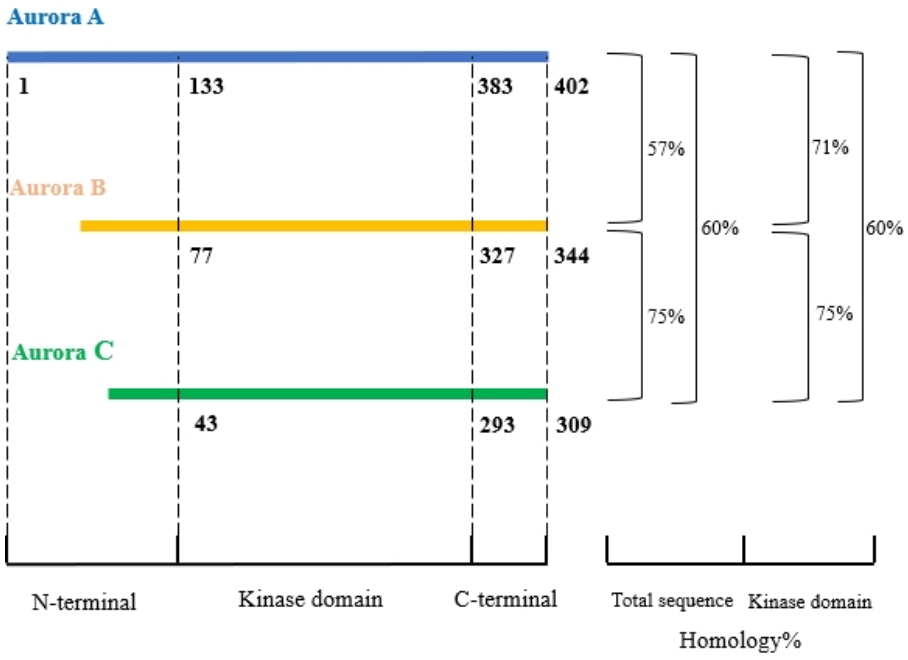

Fig. 1.4 Percentages of homology measured by sequence identity of the total amino acid sequence between Aurora A and Aurora B, Aurora A and Aurora C, Aurora B and Aurora C, respectively[56].

1.5 Expressions of Aurora Kinases in Cancer

As mentioned previously, the overexpression of Aurora kinases in diverse cancer cells makes them potent targets in cancer therapy, and finding a selective inhibitor for a specific type of Aurora kinase

is difficult yet essential. Numerous studies have demonstrated that Aurora kinase is overexpressed or amplified in various human cancers, and different somatic cancer samples, such as lung cancer, colorectal cancer, and melanoma, have been found to harbor several types of Aurora kinase mutations[58]. This indicates that Aurora kinase plays a pivotal role in cell transformation and tumorigenesis. Over the past few decades, an increasing number of studies have focused on the role of these potentially oncogenic proteins in tumor development.

Interestingly, different types of cancer exhibit varying degrees of correlation with Aurora kinases (refer to Table 1). For instance, pancreatic adenocarcinoma (PAAD), a highly lethal cancer, is notably correlated with the overexpression of Aurora A, but shows little correlation with Aurora B or C (in Fig. 1.5)[59]. Therefore, developing specific medications for PAAD by identifying inhibitors with high selectivity for Aurora A is feasible. Similarly, specific medications for various cancers can be identified and developed accordingly.

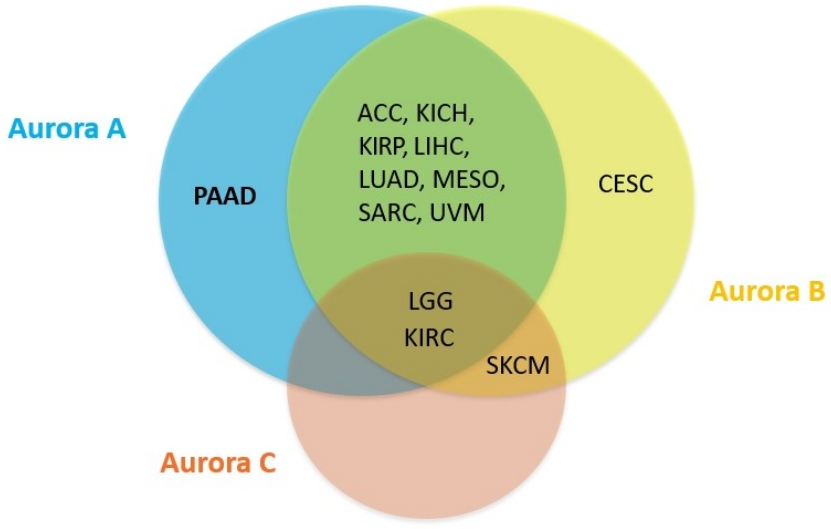

Fig. 1.5 Survival correlation among Aurora Kinases and variety of cancers

Table 1. Sensitive prognostic marker of Aurora Kinase A and B

Aurora A	Aurora B
ACC-Adrenocortical carcinoma	ACC-Adrenocortical carcinoma
LGG-Lower grade glioma	LGG-Lower grade glioma
CESC-Cervical squamous cell carcinoma	CESC-Cervical squamous cell carcinoma
KICH-Kidney chromophobe carcinoma	KICH-Kidney chromophobe carcinoma
KIRC-Kidney renal clear cell carcinoma	KIRC-Kidney renal clear cell carcinoma
KIRP-Kidney renal papillary cell carcinoma	KIRP-Kidney renal papillary cell carcinoma
LIHC-Liver hepatocellular carcinoma	LIHC-Liver hepatocellular carcinoma
LUAD-Lung adenocarcinoma	LUAD-Lung adenocarcinoma
PAAD-Pancreatic adenocarcinoma	MESO-Mesothelioma
SARC-Sarcoma	SARC-Sarcoma
UVM-Uveal melanoma	SKCM- Skin cutaneous melanoma
	UVM-Uveal melanoma

1.6 Aurora Kinase Inhibitors

Aurora kinase is closely associated with cancer development and metastasis. In recent years, there has been widespread attention on the design and development of Aurora kinase inhibitors. For instance, Aurora A is considered an oncogene that is frequently overexpressed in various human malignancies, such as colon, breast, pancreatic, and ovarian tumors[60]. The recent clinical success of kinase inhibitors in oncology has sparked significant interest in targeting Aurora kinases with small molecules. Several Aurora kinase inhibitors, exhibiting potency and selectivity over other kinases, are currently undergoing clinical trials (Fig. 1.6 and Table 2). However, only a few inhibitors demonstrate some level of subtype selectivity for either Aurora A or Aurora B[55].

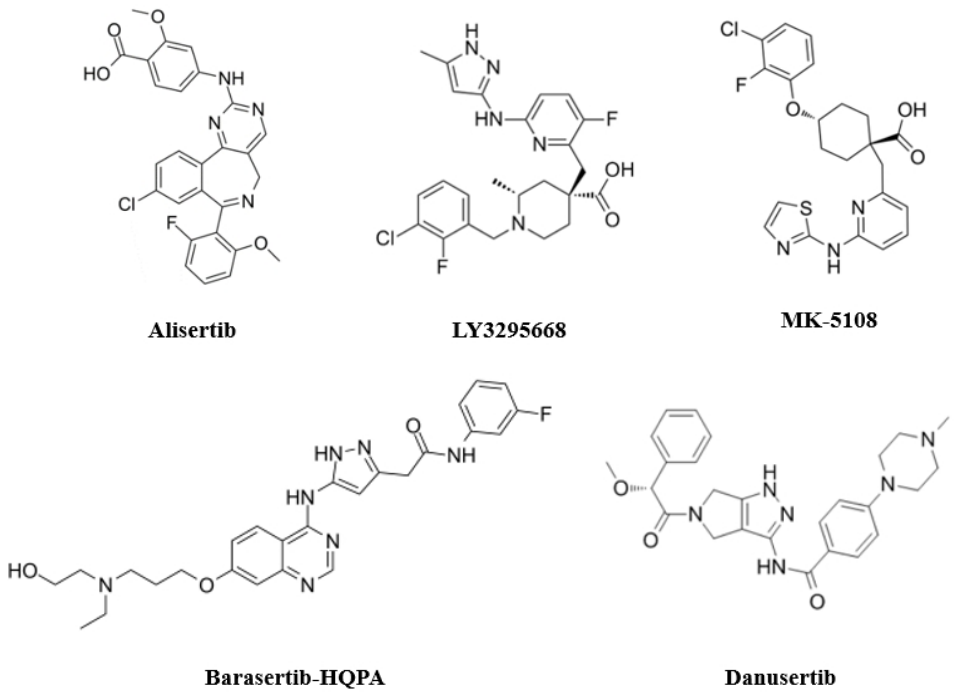

Fig. 1.6 Structures of some Aurora inhibitors

Table 2. IC_{50} of some Aurora inhibitors

Inhibitor	Aurora A (IC_{50} nM)	Aurora B (IC_{50} nM)	Aurora C (IC_{50} nM)	Current trial stage
MK-8745[56]	0.6	/	/	Preclinical
MK-5108[57]	0.064	> 15	/	I
LY3295668[58]	0.8	1038	/	I/II
TAS-119[59]	1	95	/	I
Alisertib[60]	1.2	396.5	/	I/II/III
MLN8054[61]	4	/	/	I
AKI603[62]	12.3	/	/	Preclinical
SP-96[63]	18.975	0.316	/	Preclinical
Barasertib-HPQA[64]	1368	0.37	/	I/II
Hesperidin[65]	/	250	/	Preclinical
GSK-1070916[66]	> 100	0.38	1.5	I
Danusertib[67]	13	79	61	II
BI-847325[68]	/	/	15	/

1.7 Purpose of Thesis

As mentioned earlier, understanding Aurora kinase inhibitor selectivity remains a primary objective for the design of kinase inhibitors and for clinical safety assessments. Traditional approaches for kinase selectivity analysis typically involve biochemical activity assays, binding assays, and protein-ligand crystallization. However, these methods are often prohibitively expensive and are limited by the availability of kinases. In contrast, studying kinase selectivity through molecular dynamics simulation can provide detailed insights into ligand-protein interactions, including key residues, main free energy contributions, and interaction types. Such insights can guide the design of subtype-selective inhibitors. Given the high similarity in the active site, achieving high subtype selectivity for Aurora kinase ligands is both crucial and challenging. Understanding the selective mechanisms of protein-ligand recognition at the molecular level may offer valuable insights for the rational design of selective inhibitors targeting Aurora kinase A and B, thereby helping to mitigate potential side effects.

The objective of this thesis is to elucidate the subtype selectivity mechanisms of Aurora kinase A and B by investigating several Aurora A selective inhibitors, Aurora B selective inhibitors, and inhibitors that exhibit no selectivity for either Aurora A or B. To achieve this goal, molecular docking was employed to generate complex structures. Molecular dynamics simulations were then conducted to analyze the complexes of Aurora A and B with Aurora kinase inhibitors, focusing on root mean square deviation (RMSD), average structure, binding free energy determined via MM/PBSA, and binding free energy decomposition analysis. These analyses aim to identify

favorable or unfavorable residue contributions in the active site, thereby elucidating the subtype selectivity mechanisms of Aurora kinase A and B in the presence of Aurora inhibitors.

CHAPTER TWO

EVALUATION OF AURORA A SELECTIVE INHIBITORS BINDING WITH AURORA KINASE A AND B BY MOLECULAR DYNAMICS SIMULATION

2.1 Introduction

The overexpression of Aurora kinases in various cancer cells makes them promising targets in cancer therapy. However, Aurora kinases exhibit highly conserved homology, with only four different residues present in the active site: Leu215, Thr217, Val218, and Arg220 in Aurora A (and Arg159, Glu161, Leu162, and Lys164 in Aurora B). Aurora kinases share a common catalytic core, resulting in significant sequence and structural similarities. Aurora kinase A and B, B and C, A and C share a substantial degree of identity, with over 71%, 75% and 60% similarity of sequence identity respectively[56]. These similarities in sequence and structure can contribute to a lack of selectivity and off-target toxicity of kinase inhibitors. Therefore, understanding the selectivity of Aurora kinase inhibitors remains a top priority for designing kinase inhibitors and evaluating clinical safety.

Traditional methods for analyzing kinase selectivity typically involve biochemical activity assays, binding assays, and protein-ligand crystallization. However, these approaches are costly and often limited by the availability of kinases[69]. In contrast, molecular dynamics simulation offers a means of studying kinase selectivity while also providing insights into ligand-protein interactions, such as key residues, significant free energy contributions, and interaction types.

Molecular docking predicts the preferred orientation of one molecule when bound to another to

form a stable complex[70]. Due to the lack of specific complex crystal structures, molecular docking was employed to construct the structures of Aurora A and B bound with the ligand GSK-1070619. Autodock Vina was chosen for this purpose due to its speed and accuracy[71,72].

Molecular dynamics simulation analyzes the physical movements of atoms and molecules over a fixed period of time, providing dynamic insights into the system's evolution[73]. The main steps of MD simulation include system preparation, simulation, and analysis. In this project, the Amber software package was utilized[74,75].

Molecular mechanics-generalized Born surface area (MM/GBSA) and Molecular mechanics-Poisson-Boltzmann surface area (MM/PBSA) methods are considered reliable and valid for structure-based drug design, particularly in predicting the binding affinity of a protein bound with a ligand[76]. MM/PBSA uses the Poisson-Boltzmann equation to compute the electrostatic contribution to the free-energy, while MM/GBSA uses the Generalized Born approximation, which is an approximate and faster treatment of the Poisson-Boltzmann equation[77]. MM/PBSA is deemed more accurate than MM/GBSA, and thus, MM/PBSA was employed to calculate binding free energy decomposition. The calculation results include the binding free energy contribution of each residue in the protein, aiding in identifying favorable or unfavorable residue contributions in the active site.

Comparison of ligand interactions obtained from average structures reveals differences in ligand interactions, key residues of the protein, and key functional groups of the ligand between the Aurora A and B complexes, thereby elucidating the selectivity mechanism.

2.2 Preparation of Complex Structures

As part of this research, LY3295668, MK-5108, Alisertib, GSK-1070916, and Danusertib were investigated. Specifically, LY3295668, MK-5108, and Alisertib are selective inhibitors for Aurora A, while GSK-1070916 exhibits higher selectivity for Aurora B over Aurora A. However, Danusertib was found to lack specific selectivity for either Aurora A or B.

Some complex structures can be found in the Protein Data Bank[78], while others cannot or have missing parts in the protein structure. In such cases, the proteins need to be repaired to ensure a complete structure. Additionally, structures from AlphaFold can be utilized[79,80]. AlphaFold is a computational method capable of predicting protein structures with atomic accuracy, even in cases where no similar structure is known[81]. For example, the structure of LY3295668 binding with Aurora A is based on 6C2R and corrected using AlphaFold, the structure of MK-5108 binding with Aurora A is based on 5EW9 and corrected using AlphaFold, and the structure of Danusertib binding with Aurora A is based on 2J50 and corrected using 3E5A.

To obtain sequence and structural information of Aurora proteins for comparison, sequence alignment and structure superimposition were performed. Considering the high homology and conservation of the binding site between the two Aurora proteins, the interaction modes of LY3295668, MK-5108, and Danusertib with Aurora A and Aurora B are expected to be very similar. Therefore, it is not optimal to rebuild the binding models using molecular docking methods. Instead, a straightforward and reliable approach is to align and merge based on the similar binding modes of LY3295668, MK-5108, and Danusertib with homologous Aurora kinases[82].

There are no crystal structures related to GSK-1070916 binding with human Aurora kinases. Molecular docking was thus employed to predict the initial structure of the GSK-1070916/Aurora A model and the GSK-1070916/Aurora B model. Specifically, even though the crystal structure of the inhibitor GSK-1070916 is unavailable, it can be drawn and adjusted using ChemDraw.

Research indicates that the active conformation of Aurora kinases is the lowest energy state compared to the inactive conformation and the active conformation with partner protein. As mentioned earlier, Aurora C primarily functions in germ cells and has minimal correlation with cancer. Therefore, this study only focuses on the active conformations of Aurora A and Aurora B. The resources of the ligand, protein, and complex in each system are summarized in Table 3.

More significantly, regardless of how the protein-ligand complex was obtained, they were all optimized by MD simulation.

Table 3. Resources of the ligand, protein and building method of the starting structure in each system.

		LY-3295668	MK-5108	Alisertib	GSK-1070916	Danusertib
Aurora A	Ligand	6C2R	5EW9	3E5A	Chemdraw	2J50
	Protein	6C2R, AlphaFold	5EW9, AlphaFold	2X81	AlphaFold	2J50, 3E5A
	Complex	Crystal structure	Crystal structure	Crystal structure	Docking	Crystal structure
Aurora B	Ligand	6C2R	5EW9	5IA0	ChemDraw	2J50
	Protein	AlphaFold	AlphaFold	AlphaFold	AlphaFold	AlphaFold
	Complex	Crystal structure	Crystal structure	Crystal structure	Docking	Crystal structure

AlphaFold database access ID:

AF-A3KFJ2-F1 (Homo sapiens Aurora kinase A)

AF-A0A3D4H337-F1 (Homo sapiens Aurora kinase B)

2.3 Molecular Docking

Molecular docking involves studying how two or more molecular structures, such as a drug and an enzyme or protein, fit together. It predicts the preferred orientation of one molecule when bound to another to form a stable complex[83]. The method aims to identify the correct poses of ligands in the binding pocket of a protein and predict the affinity between the ligand and the protein. Docking can be classified into protein-small molecule (ligand) docking, protein-nucleic acid docking, and protein-protein docking, depending on the types of ligands[84,85]. In this study, docking is employed to predict how the protein interacts with small molecules (ligands).

Docking involves placing rigid molecules or fragments into the active site of a protein using various methods, such as pose clustering. The performance of docking relies on search algorithms like the Monte Carlo method, genetic algorithm, fragment-based method, and distance geometry method, as well as scoring functions like the force field method and empirical free energy scoring function[86]. The first step in docking is to generate a composition of all possible conformations and orientations of the protein paired with the ligand. Then, the score function calculates a number indicating favorable interaction[87]. The active site of the protein can be identified by selecting the required crystal structure from the Protein Data Bank (PDB) and extracting the bound ligand, which optimizes the protein's active site of interest[88]. When the bound ligand is absent in the crystal structure, identifying the active site in a protein becomes critical. In such cases, a comprehensive literature review of the source papers from which the crystal structure in the PDB is obtained can help identify the active site residues. If an existing drug has the same pharmacological effect on a protein, the drug's active site should be determined. In the initial stages of analysis, these residues

can be considered as active binding sites for test ligands[89].

Due to the lack of complex crystal structures, molecular docking was performed to construct the structures of Aurora A and B bound with the ligands[90]. Autodock Vina was chosen for this task due to its speed and accuracy. The initial structures of the GSK-1070916/Aurora A model and the GSK-1070916/Aurora B model were generated using molecular docking in the AutoDockTools 1.5.6 program[71,72]. A cubic box of 25 Å × 25 Å × 25 Å was defined, with the ATP-binding sites as the center and a grid spacing of 0.3 Å. Gasteiger partial charges were distributed to the atoms of GSK-1070916 using the AutoDockTools program. AutoGrid software was used to estimate the affinity maps of Aurora A[91]. The docking parameters were set as follows: 300 docking trials, clustering according to the RMSD tolerance of 1.0 Å, maximum number of evaluations set to 25,000,000, and other parameters set to default values. The highest-ranking structures for the GSK-1070916/Aurora A and GSK-1070916/Aurora B models were selected for the next step of molecular dynamics (MD) simulation.

2.4 Molecular Dynamics Simulation

Molecular dynamics (MD) simulation is a computational method for analyzing the physical movements of atoms and molecules. It operates within the framework of classical mechanics and numerically simulates the motion of molecular systems[92]. Molecular dynamics simulation enables the simulation of chemical and physical processes on computers, providing kinetic information on a microscopic scale, offering theoretical support for experiments, and guiding chemical

experiments[93,94]. Since molecular systems typically involve a large number of particles, determining the properties of such complex systems analytically is impractical. MD simulations circumvent this issue by employing numerical methods. Additionally, computational simulations can help reduce the costs associated with manual experiments. MD simulations can also be conducted under specific conditions, such as ultra-high pressure, ultra-high temperature, strong electric fields, and strong magnetic fields[95].

MD simulations were performed using AMBER 18. The force field FF98SB was used for proteins, whereas GAFF was used for non-peptide components of the system, including the small organic compounds[96]. Water molecules were added using the TIP4P model around the molecular models, with a 9 Å buffer from the edge of the periodic box. Counter ions were introduced to achieve total charge neutrality. The atomic charges of protein come from force field; while atomic charges of ligand come from a charging scheme employed, the net charge set before MD depend on the ligand protonation state at pH of 7.4.

The system underwent equilibration through three steps[55]:

Prior to molecular dynamics simulation, energy minimization was performed to relax the complex systems. During the minimization step, the system underwent relaxation through 5000 steps of steepest descent followed by 3000 conjugate gradient minimization steps, with a force constant of 10.0 kcal mol·$Å^{-2}$ applied to the protein and ligand. This process was repeated two more times with a force constant of 10.0 kcal mol·$Å^{-2}$ applied to the protein and ligand respectively.

In the second step, the system was heated in two sequential runs to 300 K, while maintaining a

force constant of 10.0 kcal mol·Å^{-2} on the protein. Initially, the system was rapidly heated to 100 K, followed by a gradual increase until reaching 300 K. The constant-temperature, constant-pressure ensemble (NPT) was utilized during this step. Temperature control was achieved using a Langevin thermostat with a collision frequency of 1.0 ps^{-1}.

In the final step, an NTP MD simulation was conducted for 5 ns with a time step of 2 fs and a force constant of 5.0 kcal mol·Å^{-2} applied to the protein for equilibration.

Following the equilibration run, each system was simulated for more than 300 ns using the NPT ensemble. Temperature regulation was maintained using a Berendsen Thermostat. All simulations were conducted with periodic boundary conditions. The SHAKE algorithm was applied to all atoms covalently bonded to hydrogen atoms[97]. Long-range electrostatic interactions were calculated using the particle mesh Ewald (PME) method. Non-bond interactions were treated with a residue-based cutoff of 10 Å[75,98].

2.5 RMSD and Average Structure

Root-mean-square deviation (RMSD) was employed to assess the dynamic stability of the complex and ascertain whether the ligand deviated from the protein[99]. The RMSDs of the protein backbone and mwRMSDs (mass-weighted) of ligand molecules from the initial structure were analyzed across all MD trajectories. To scrutinize conformational changes, the averaged structures derived from MD simulations were compared with the crystal structures. The averaged structures for all atoms were computed using the CPPTRAJ module of AMBER 18 from the final 120 ns simulation

trajectories, excluding water and ions, with a sampling interval of 0.5 ns[75]. After 50ns, the curve fluctuates within a very narrow range, which can be regarded as stabilizing. After that, the average structures are very similar. Subsequently, these structures underwent minimization to alleviate unrealistic bonds and angles. The distances between the center of mass of atoms were calculated using the same module and parameters.

Analyzing the average structures of these models facilitated the extraction of information regarding the residues engaged in ligand interactions and the types of interactions involved, which proved invaluable for subsequent analyses. Moreover, the average structures exhibited minimal alteration when compared to the initial structures by superimposing the structures, suggesting that, at this juncture, the initial structures could be deemed reasonable. Some of the structures were modeled in various ways and one of them was obtained by molecular docking. Even if the overall shape of the protein (as measured by RMSD between Carbon alpha or backbone atoms) did not change much, intermolecular interactions would have been significantly optimized after MD reached equilibrium.

2.6 Binding Free Energy Calculation

Molecular mechanics-generalized Born surface area (MM/GBSA) and Molecular mechanics-Poisson-Boltzmann surface area (MM/PBSA) are regarded as reliable and valuable techniques for structure-based drug design. This is owing to their exceptional capability to predict the binding affinity between a protein and its ligand[100]. By assessing the efficacy of MM/GBSA and MM/PBSA

in predicting binding free energies, it was observed that MM/PBSA outperformed MM/GBSA in calculating absolute binding free energies, though not necessarily relative binding free energies[101,102]. MM/GBSA can serve as a potent tool in drug design, where correct ranking of inhibitors is often emphasized, considering its computational efficiency[103].

The binding free energy of each system was calculated using the MMPBSA.py program in AMBER 18, which conducts both MMPBSA and MMGBSA calculations[75]. This method involves post-processing, utilizing representative snapshots from a conformational ensemble to determine the free energy change between two states, typically the bound and free states of a receptor and ligand. Free energy differences are computed by amalgamating gas phase energy contributions, which remain independent of the chosen solvent model, alongside solvation free energy components (both polar and non-polar) determined from an implicit solvent model for each species[104,105]. Further refinement may include adding entropy contributions to the total free energy.

A total of 240 snapshots were extracted from each 120 ns trajectory at intervals of 0.5 ns. Prior to analysis, all water molecules and counter ions were removed from the trajectories. For each snapshot, the free energy was computed using the following equation[106]:

$$\Delta G_{bind} = G_{complex} - \left[G_{ligand} + G_{protein}\right] \quad (1)$$

Where $G_{complex}$, G_{ligand} and $G_{protein}$ were the free energies for the complex, ligand and protein, respectively. Each of them was summed with the following equations:

$$\Delta G_{bind} = \Delta G_{MM} + \Delta G_{solv} - T\Delta S \quad (2)$$

$$\Delta G_{bind} = (\Delta G_{elec} + \Delta G_{vdw}) + (\Delta G_{pb} + \Delta G_{np}) - T\Delta S \quad (3)$$

The binding free energy (ΔG_{bind}) in equation 2 is calculated from a sum of the changes in the molecular mechanical (MM) gas-phase binding energy (ΔG_{MM}), the solvation free energy (ΔG_{solv}) and entropic contribution ($T\Delta S$) at temperature T. ΔG_{MM} is the sum of gas phase coulomb interaction (ΔG_{elec}) and van der Waals interaction (ΔG_{vdw}) energies. The solvation free energy (ΔG_{solv}) is the sum of polar contribution to solvation (ΔG_{pb}) and nonpolar solvation term ΔG_{np}. The polar solvation energy was calculated by solving the Poisson-Boltzmann (PB) equation. The values of dielectric constant of the surrounding solvent molecules and the solute were set to 80 and 1. Specifically, the dielectric constant of water is 80, and the dielectric constant of a vacuum is considered to be 1.0 The nonpolar solvation term was computed using the following equation:

$$\Delta G_{np} = \gamma \Delta SASA + b,^{107} \quad (4)$$

where γ was the surface tension that was set to 0.0072 kcal/ (mol Å^2), and b was a constant set to 0. SASA is the solvent-accessible surface area (Å^2) that was estimated using the MOLSURF algorithm. The solvent probe radius was set to 1.4 Å to define the dielectric boundary around the molecular surface.

2.7 Binding Free Energy Decomposition

To elucidate the intricate interactions between the protein and ligand, the binding free energy was decomposed for each residue. As previously mentioned, MM/PBSA is deemed a more accurate method compared to MM/GBSA. Hence, MM/PBSA was employed to compute the binding free energy decomposition[108,109]. However, MM/GBSA calculation is faster and also a reliable method.

Comparing the results from MM/GBSA and MM/PBSA can verify their correctness and improve the reliability. The results of the calculations included the contribution of binding free energy from each residue within the protein. This allowed for the identification of favorable or unfavorable residue contributions within the active site[110-113]. In comparison to the ligand interactions deduced from the average structures, this analysis could delineate the distinctions in ligand interactions, key residues within the protein, and crucial functional groups of the ligand across the complexes of Aurora A, B, and C. Consequently, it facilitated the elucidation of the selectivity mechanism of Aurora kinases.

2.8 Results and Discussion

2.8.1 LY3295668, MK-5108 and Alisertib

Build the systems

The crystal structure of Human Aurora A binding with LY3295668 was retrieved from PDB: 6C2R, but the protein was not complete, so the missing residues on activation loop had to be fixed by homology modeling based on the templates of 6C2R and the structure retrieved from AlphaFold Protein Structure Database[78], the AlphaFold database access ID is AF-A3KFJ2-F1. Due to the lack of crystal structure of LY3295668 binding with human Aurora B, the active Aurora B was retrieved from AlphaFold Protein Structure Database: Homo sapiens Aurora kinase B[79,80], the AlphaFold database access ID is AF-A0A3D4H337-F1. The all-atom accuracy of AlphaFold was 1.5 Å RMSD95 (95% confidence interval = 1.2–1.6 Å) compared with the 3.5 Å r.m.s.d.95 (95%

confidence interval = 3.1–4.2 Å) of the best alternative prediction method. Since the existing human Aurora A/LY3295668 (6C2R) was fixed and the highly conserved homology between Aurora kinase A and B mentioned before, the human Aurora B was superimposed structurally to the complete Aurora A/LY3295668 complex instead of rebuilding the binding models by molecular docking methods. Then the ligand conformation was extracted from the template and merged into the target models. Significantly, the net charge of LY3295668 was set to 0 when preparing the systems due to its protonation state at the pH of 7.4. The starting structures of LY3295668/Aurora A and LY3295668/Aurora B models are shown in Fig. 2.1.

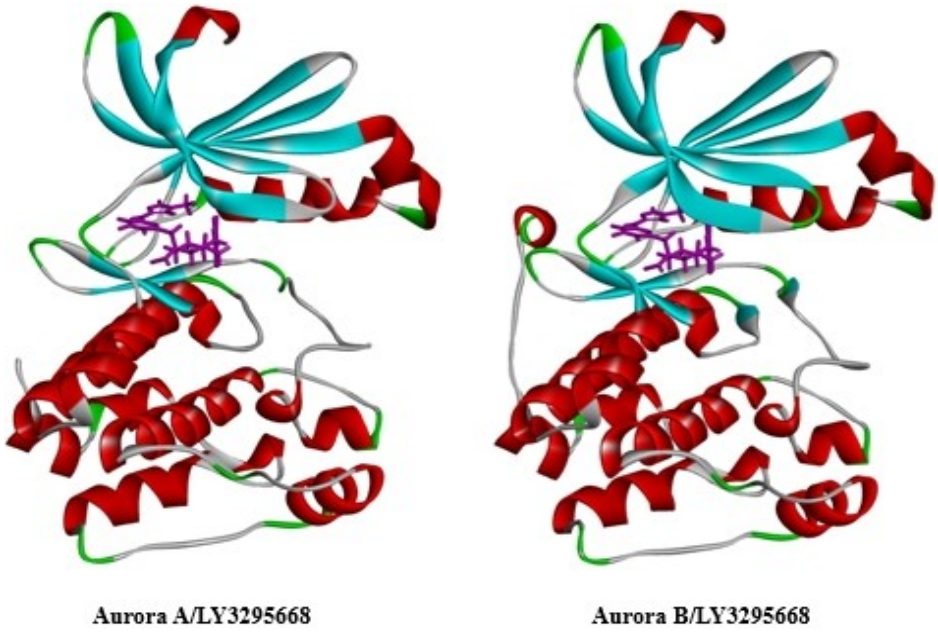

Fig. 2.1 Starting structures of Aurora kinase A and B binding with LY3295668.

The process of building the starting structures of Aurora kinase A and B with MK-5108 was similar to LY3295668. The crystal structures of Human Aurora A binding with MK-5108 was retrieved

from PDB: 5EW9, and then fixed based on the templates of 5EW9 and the structure retrieved from AlphaFold Protein Structure Database, the AlphaFold database access ID is AF-A3KFJ2-F1. The human Aurora B was retrieved from AlphaFold Protein Structure Database: Homo sapiens Aurora kinase B, the AlphaFold database access ID is AF-A0A3D4H337-F1. The human Aurora B was superimposed structurally to the complete Aurora A/MK-5108 complex, and then the ligand conformation was extracted from the template and merged into the target models. Significantly, the net charge of MK-5108 was set to -1 when preparing the systems due to its protonation state at the pH of 7.4. The starting structures of MK-5108/Aurora A and MK-5108/Aurora B models are shown in Fig. 2.2.

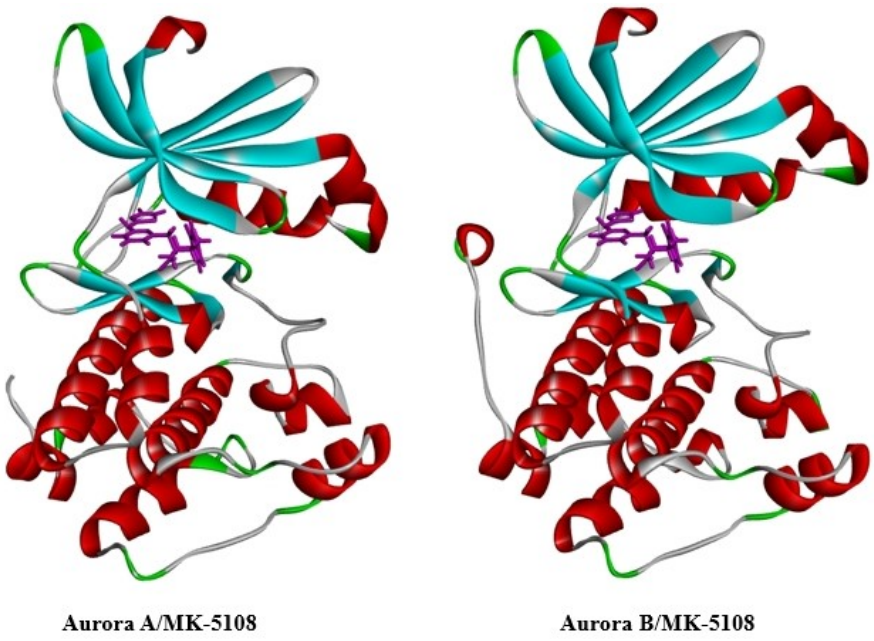

Fig. 2.2 Starting structures of Aurora kinase A and B binding with MK-5108.

The models were constructed by structurally superimposing the crystal structure of Aurora A (3E5A)

and the AlphaFold structure of Aurora B to the crystal complex of Aurora A-MLN8054 (PDB ID: 2X81) due to the similar structure of Alisertib to MLN8054 (Fig. 2.3). Then the moieties were modified on MLN8054 to get Alisertib (Fig. 2.4). Significantly, the net charge of Alisertib was set to -1 when preparing the systems due to its protonation state at the pH of 7.4.

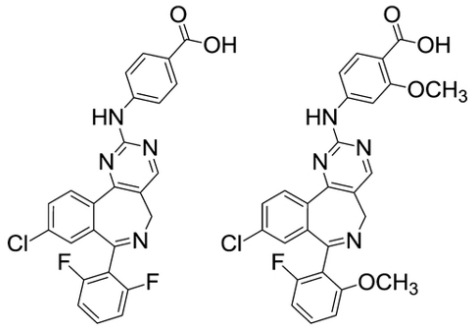

Fig. 2.3 The structure of Alisertib and MLN8054.

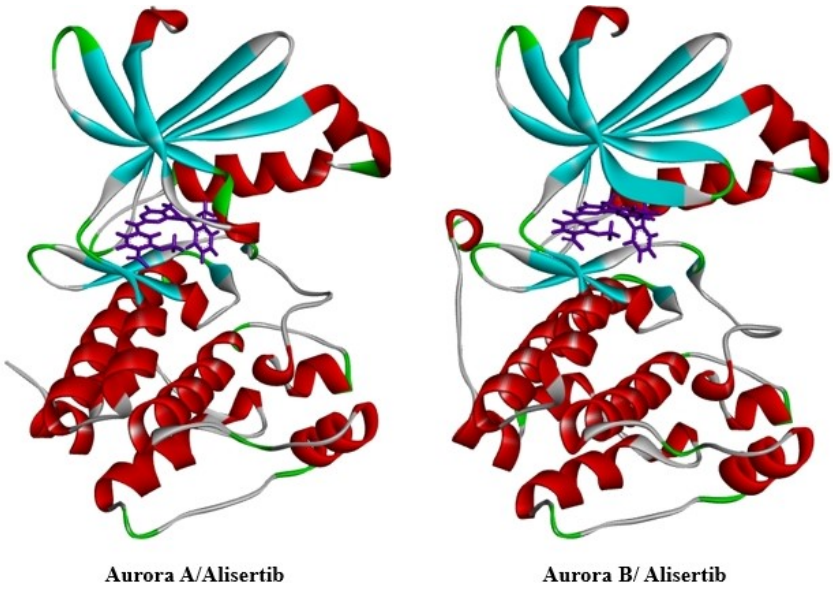

Fig. 2.4 Starting structures of Aurora kinase A and B binding with Alisertib.

Stability of complex models and ligand interactions

To assess the dynamic stability of the complexes and validate the rationality of the sampling method used during the 50 ns MD simulation for each complex, root-mean-square deviations (RMSD) from the starting structure were analyzed. As depicted in Fig. 2.5, Fig. 2.6 and Fig. 2.7, this analysis indicated that the proteins, active sites, and ligands in these systems remained stable after reaching equilibrium.

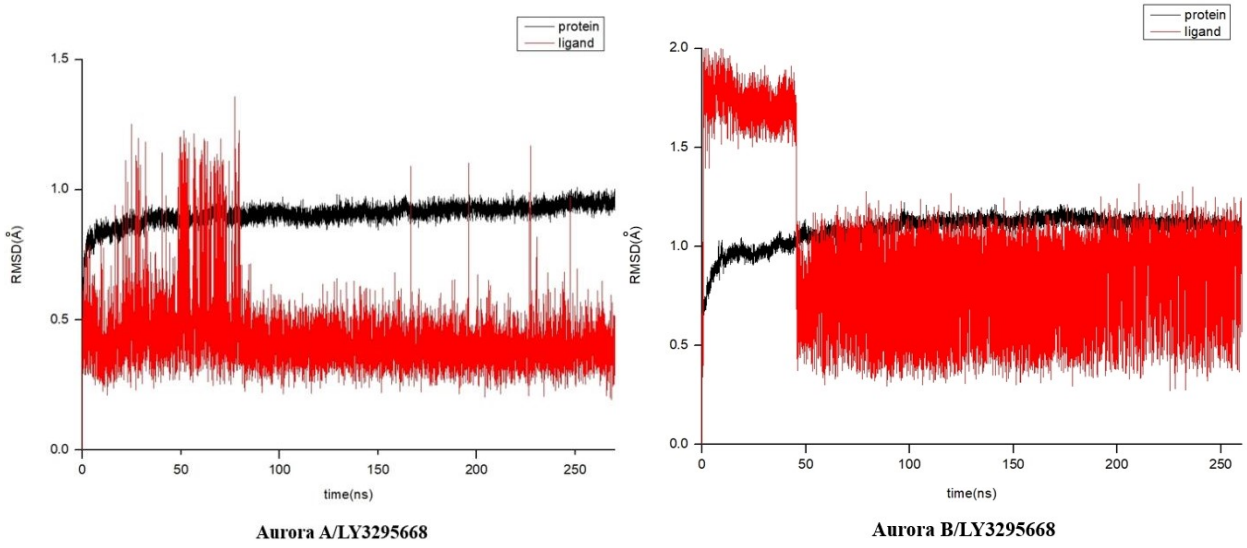

Fig. 2.5 The root mean square deviation (RMSD) of Aurora kinase A and B binding with LY3295668.

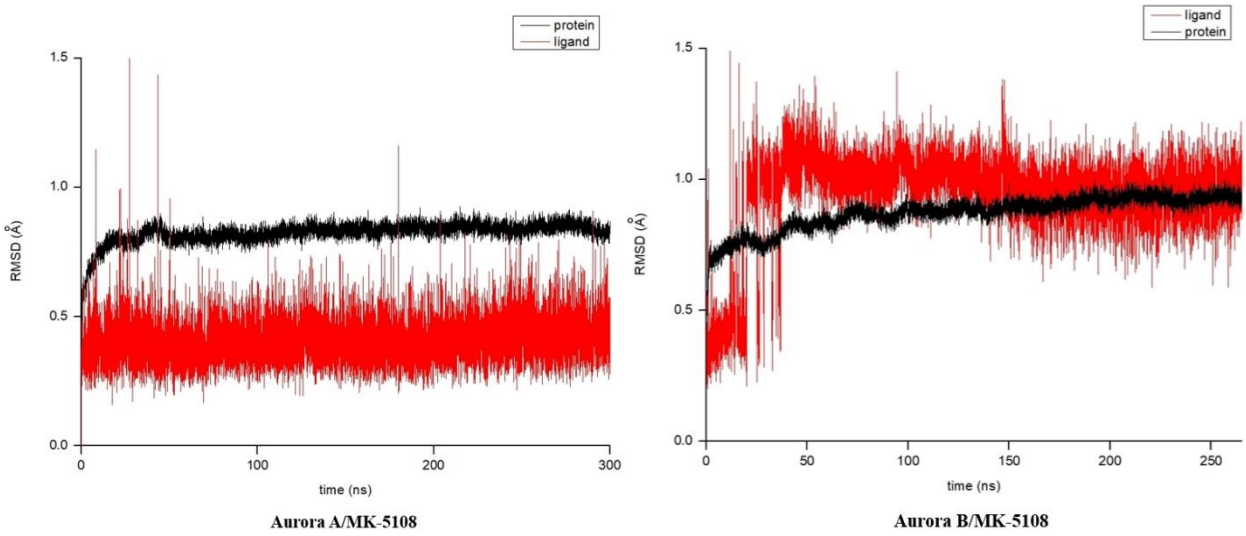

Fig. 2.6 The root mean square deviation (RMSD) of Aurora kinase A and B binding with MK-5108.

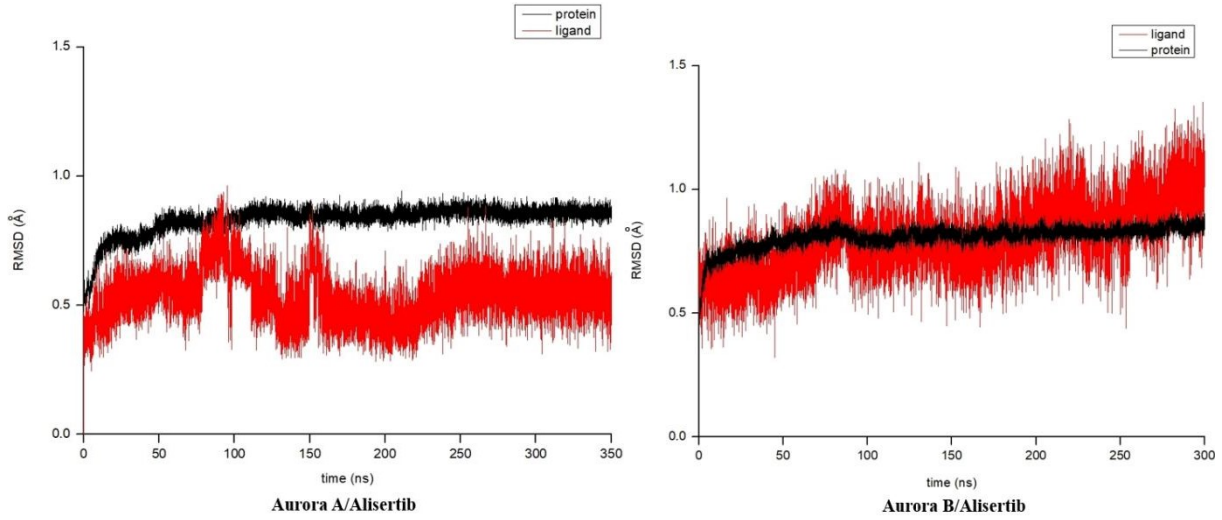

Fig. 2.7 The root mean square deviation (RMSD) of Aurora kinase A and B binding with Alisertib.

According to the average structure and ligand interactions of LY3295668 binding with Aurora A and B, LY3295668 was stabilized in the binding pocket formed by residues Arg137, Leu139, Phe144, Ala160, Lys162, Leu194, Glu211, Ala213, Gly216, Thr217, Arg220, Leu263 and Ala273 for Aurora A; Arg81, Leu83, Ala104, Leu138, Glu155, Ala157, Gly160, Glu161, Leu207 and Ala217 for Aurora B (Fig. 2.8).

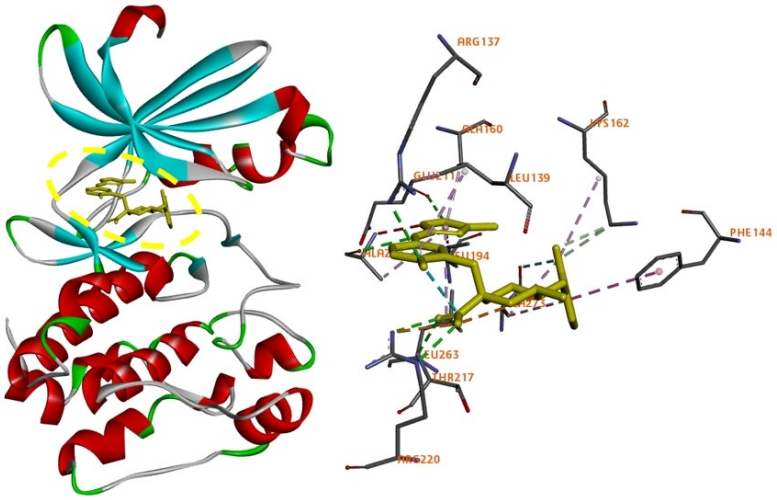

Aurora A/LY3295668

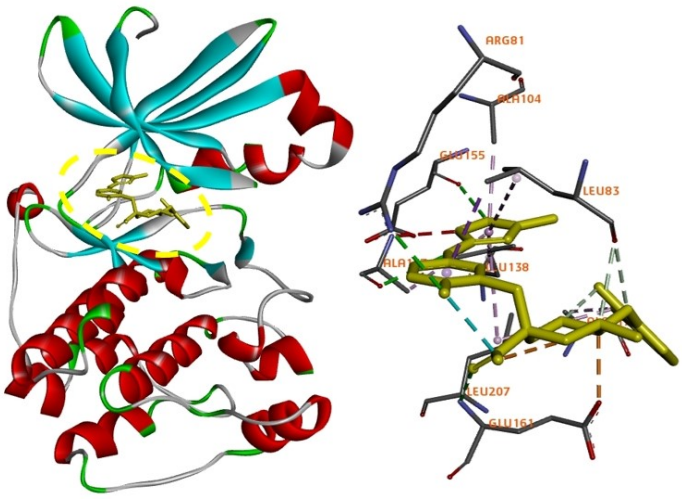

Aurora B/LY3295668

Fig. 2.8 Average structures and ligand interactions of Aurora kinase A and B binding with LY3295668.

According to the average structure and ligand interactions of MK-5108 binding with Aurora A and B, MK-5108 was stabilized in the binding pocket formed by residues Leu139, Val147, Ala160, Lys162, Leu194, Leu210, Glu211, Ala213, Thr217, Arg220, Leu263 and Ala273 for Aurora A; Arg81, Leu83, Ala104, Leu154, Tyr156, Ala157, Ala164, Leu207 and Ala217 for Aurora B (Fig. 2.9).

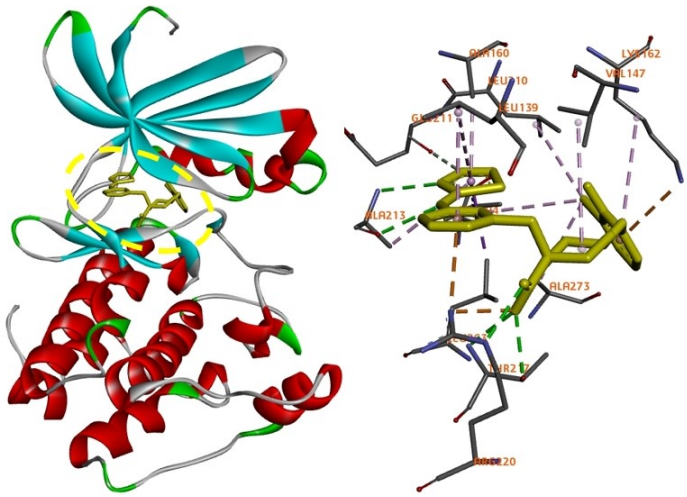

Aurora A/MK-5108

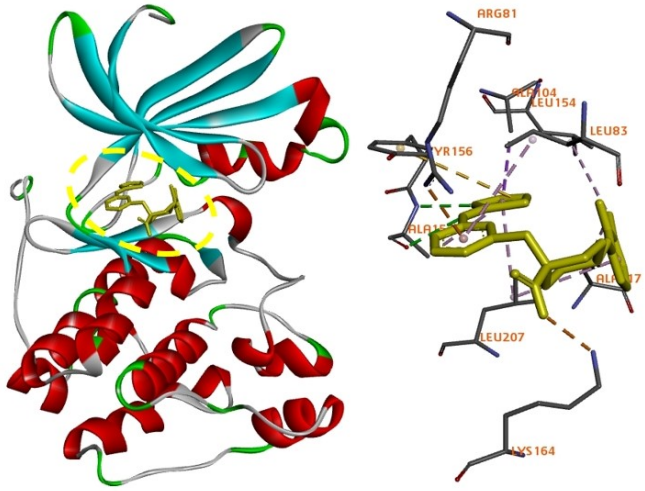

Aurora B/MK-5108

Fig. 2.9 Average structures and ligand interactions of Aurora kinase A and B binding with MK-5108.

According to the average structure and ligand interactions of Alisertib binding with Aurora A and B, Alisertib was stabilized in the binding pocket formed by residues Arg137, Leu139, Phe144, Val147, Ala160, Lys162, Glu181, Glu211, Ala213, Glu260, Leu263 and Ala273 for Aurora A; Arg81, Leu83, Val91, Ala104, Ala157, Glu161, Glu204, Leu207 and Ala217 for Aurora B (Fig. 2.10).

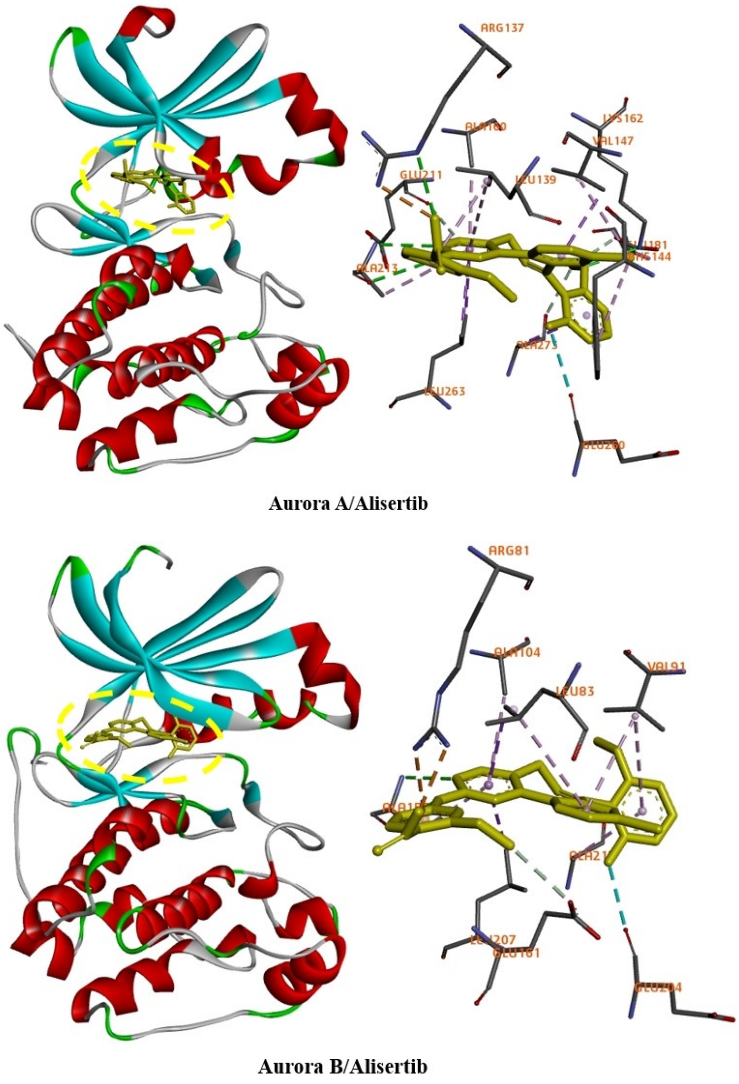

Fig. 2.10 Average structures and ligand interactions of Aurora kinase A and B binding with Alisertib.

Binding free energy calculations

The calculated binding free energies of Aurora A/LY3295668 and Aurora B/LY3295668 are presented in Table 4, along with the contributions of their components calculated using the MM/PBSA and MM/GBSA methods. It is evident that the energy rankings predicted by both methods are highly consistent, with the free energy value obtained from MM/PBSA being lower than that from MM/GBSA. It is important to note that while the binding free energies calculated with MM/PBSA and MM/GBSA may not precisely match the absolute experimental values, they have demonstrated a strong correlation with experimental results.

The results show that the Van der Waals energy, polar solvation energy, and nonpolar solvation energy favor binding in all systems,since these values are negative. While the electrostatic interaction contribution in vacuum shows an unfavorable contribution. However, the favorable polar solvation energy is offset by the unfavorable electrostatic energy resulting in disadvantages. Van der Waals and nonpolar solvation energies are often closely related to hydrophobic interactions, which are responsible for burying the hydrophobic groups of the ligand into the receptor binding pocket. The sum of Van der Waals energy and nonpolar solvation energy contributes favorably to all four complex systems, indicating that hydrophobic interactions are the main driving force for the binding of LY3295668 to Aurora A and B. The summation of $\Delta G_{vdw} + \Delta G_{np}$ is much more favorable for the Aurora B model with the binding free energy of -58.76 kcal/mol than for the Aurora A model with the binding free energy of -55.04 kcal/mol. However, the $\Delta G_{ele} + \Delta G_{pb}$ sum of the Aurora B model with the binding free energy of 22.06 kcal/mol is more unfavorable than the

Aurora A model with the binding free energy of 9.88 kcal/mol, making the overall enthalpy contribution favor the binding of LY3295668 to Aurora A. Overall, hydrophobic interactions are an important driving force for the binding of LY3295668 to Aurora A and B. Changes in electrostatic and polar solvation interactions primarily differentiate the binding affinities of Aurora A and B for LY3295668.

The same method can be used to obtain the binding free energies of MK-5108 and Alisertib. It can be found that MK-5108 and Alisertib are Aurora A selective inhibitors, which are in line with experimental correlations from IC_{50} data (in Table 5).

Table 4. The binding free energy and the contributions of its components for LY3295668 with Aurora A and B calculated from MM/PBSA and MM/GBSA method (kcal/mol)

System	Aurora A/LY3295668	Aurora B/LY3295668
ΔG_{vdw}	-50.90±0.29	-54.47±0.30
ΔG_{ele}	-97.27±0.51	-66.24±0.58
ΔG_{pb}	108.40±0.36	88.30±0.50
ΔG_{np}	-4.14±0.01	-4.30±0.01
ΔG_{MM}	-148.16±0.47	-120.71±0.58
ΔG_{solv}	104.26±0.36	84.00±0.50
ΔG_{PB}	-43.90±0.35	-36.70±0.54

System	Aurora A/LY3295668	Aurora B/LY3295668
ΔG_{vdw}	-50.90±0.29	-54.47±0.30
ΔG_{ele}	-97.27±0.51	-66.24±0.58
ΔG_{gb}	89.99±0.35	76.12±0.48
ΔG_{surf}	-6.70±0.02	-6.60±0.02
ΔG_{MM}	-148.16±0.47	-120.71±0.58
ΔG_{solv}	83.30±0.35	69.52±0.48
ΔG_{GB}	-64.87±0.33	-51.19±0.38

ΔG_{vdw} is the Van der Waals contribution from the MM force field.

ΔG_{ele} is the electrostatic interaction calculated with the MM force field.

ΔG_{pb} is the electrostatic contribution to the solvation energy calculated by the PB approach.

ΔG_{np} is the nonpolar contribution to the solvation energy.

ΔG_{surf} is the nonpolar solvation energy from MMGBSA.

ΔG_{MM} is the gas phase energy ($\Delta G_{vdw} + \Delta G_{ele}$).

ΔG_{solv} is the total solvation energy ($\Delta G_{pb} + \Delta G_{np}$).

$\Delta G_{PB} = \Delta G_{vdw} + \Delta G_{ele} + \Delta G_{pb} + \Delta G_{np}$

ΔG_{gb} is the electrostatic contribution to the solvation energy calculated by the GB approach.

$\Delta G_{GB} = \Delta G_{vdw} + \Delta G_{ele} + \Delta G_{gb} + \Delta G_{surf}$

Table 5. The binding free energy of Aurora kinase A and B with LY3295668, MK-5108 and Alisertib calculated from MM/PBSA and IC_{50}.

System	ΔG_{PB} (kcal/mol)	IC_{50} (nM)
Aurora A/LY3295668	-43.90	0.8
Aurora B/LY3295668	-36.71	1038
Aurora A/MK-5108	-55.22	0.064
Aurora B/MK-5108	-32.14	> 15
Aurora A/Alisertib	-44.37	1.2
Aurora B/Alisertib	-36.90	396.5

Mechanisms of selectivity for LY3295668, MK-5108 and Alisertib over Aurora kinase A and B

To investigate the selectivity mechanism of LY3295668, per-residue free energy decomposition was applied to the Aurora A and B models. Residues exhibiting binding free energies lower than –1 kcal/mol are typically regarded as key contributors to ligand binding, as depicted in Fig. 2.11. In the LY3295668/Aurora A model, the key residues for the binding with LY3295668 are mainly Leu139, Glu211, Tyr212, Ala213, Gly216, Thr217, Arg220 and Leu263 with the binding free energy lower than –1 kcal/mol. Arg220 forms the strongest interaction with the ligand (-7.99 kcal/mol) through multiple interactions including a hydrogen bonding interaction with the hydroxyl (single-bonded OH) on the carboxylate group of the ligand and an attractive charge interaction with

the carbonyl (double bonded O) on the carboxylate group of the ligand (Fig. 2.12). The residues Arg137, Lys162, Glu260 and Ala273 contribute unfavorably to the binding of LY3295668 in Aurora A, as indicated by their positive binding free energies. The most unfavorable interaction is generated by Lys162, with the binding free energy of 4.95 kcal/mol. The ligand-residue interaction types of LY3295668 with Aurora A are listed in Table 6, only the residues with energy contributions over 1.0 kcal/mol or under -1.0 kcal/mol are shown.

In LY3295668/Aurora B model, the key residues for the binding with LY3295668 are mainly Leu83, Glu155, Tyr156, Ala157, Gly160, Lys164 and Leu207 with the binding free energy lower than –1 kcal/mol (Fig. 2.13). Tyr156 forms the strongest interaction with the ligand (-2.54 kcal/mol). The residues Glu161 and Glu204 contribute unfavorably to the binding of LY3295668 in Aurora B, as indicated by their positive binding free energies, with the binding free energy of 4.48 kcal/mol and 4.89 kcal/mol. The ligand-residue interaction types of LY3295668 with Aurora B are listed in Table 7, only the residues with energy contributions over 1.0 kcal/mol or under -1.0 kcal/mol are shown.

In the binding site of Aurora A, Thr217 and Arg220 show great contributions to the binding with the ligand, with the binding free energy of -2.44 kcal/mol and -7.99 kcal/mol. However, in the binding site of Aurora B, Lys164 (Arg220 in Aurora A) only contributes the binding free energy of -1.98 kcal/mol, Glu161 (Thr217 in Aurora A) even shows a strong unfavorable binding free energy contribution (4.48 kcal/mol) through salt bridge interaction. The significant disparities in binding free energy observed for Thr217/Glu161 and Arg220/Lys164 in Aurora A compared to Aurora B account for the selectivity variation when LY3295668 binds to Aurora kinases. Consequently,

Thr217 and Arg220 emerge as pivotal residues in Aurora A's interaction with the ligand LY3295668, rendering LY3295668 a highly selective inhibitor of Aurora A. Additionally, the carboxylate functional group of the inhibitor plays a crucial role in driving the selectivity differences observed in ligand interactions.

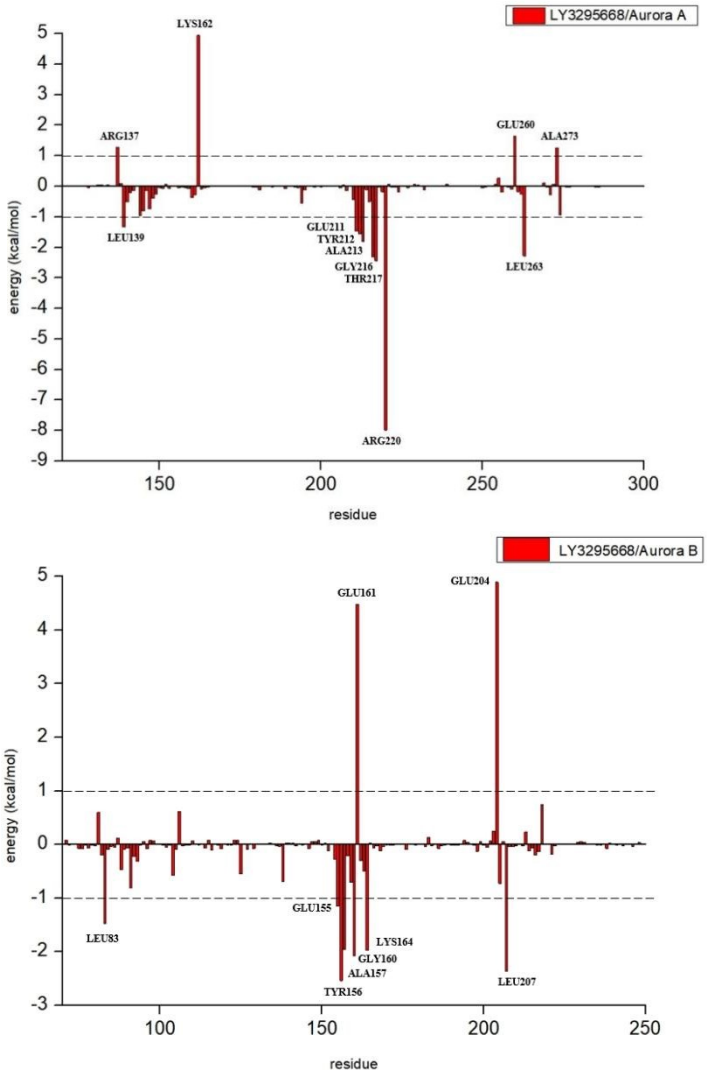

Fig. 2.11 Ligand-residue interaction energies from the MM/PBSA energy decomposition for LY3295668 with Aurora A and B. The residues with energy contributions over 1.0 kcal/mol and under -1.0 kcal/mol or labeled.

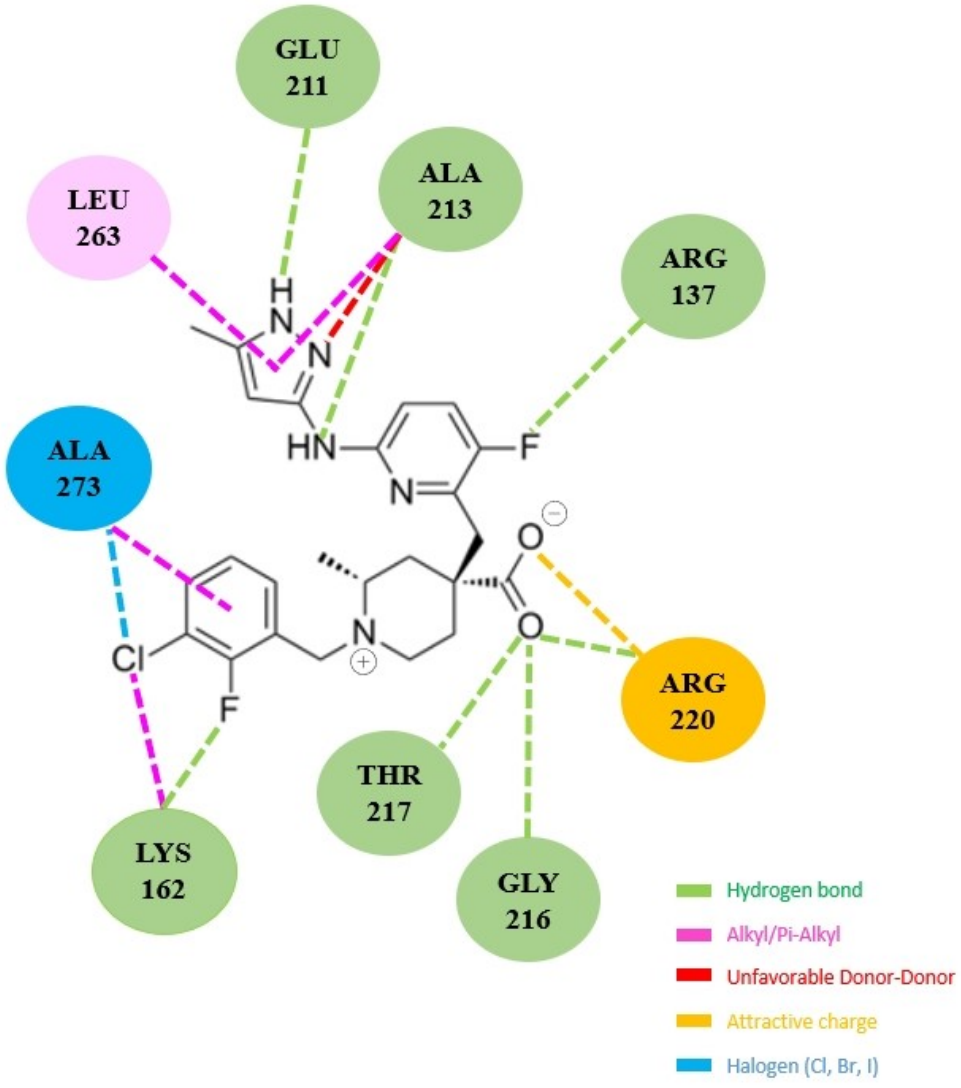

Fig. 2.12 Ligand-residue interactions of LY3295668 with Aurora A. Only the residues with energy contributions over 1.0 kcal/mol or under -1.0 kcal/mol are shown.

Table 6. Ligand-residue interaction types of LY3295668 with Aurora A. Only the residues with energy contributions over 1.0 kcal/mol or under -1.0 kcal/mol are shown.

Residue	Number	Interaction type
ARG	137	Hydrogen Bond
LYS	162	Hydrogen Bond Alkyl
GLU	211	Hydrogen Bond
ALA	213	Hydrogen Bond Unfavorable Donor-Donor Pi-Alkyl
GLY	216	Hydrogen Bond
THR	217	Hydrogen Bond
ARG	220	Attractive charge Hydrogen Bond
LEU	263	Pi-Alkyl
ALA	273	Halogen (Cl, Br, I) Pi-Alkyl

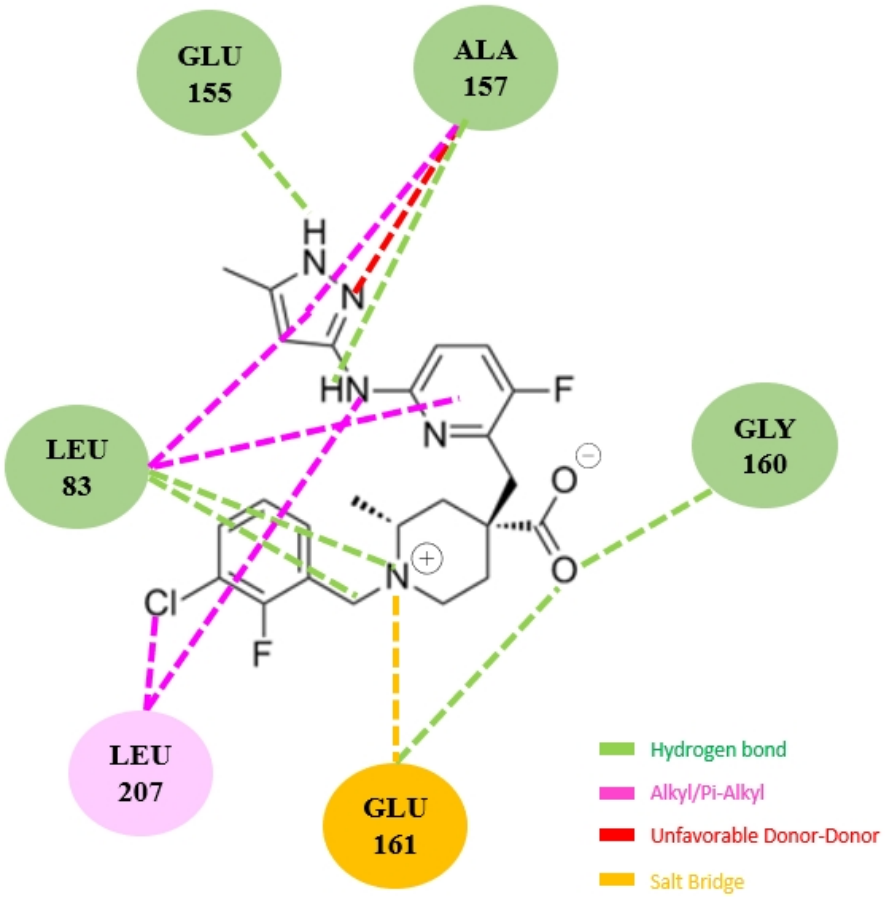

Fig. 2.13 Ligand-residue interactions of LY3295668 with Aurora B. Only the residues with energy contributions over 1.0 kcal/mol or under -1.0 kcal/mol are shown.

Table 7. Ligand-residue interaction types of LY3295668 with Aurora B. Only the residues with energy contributions over 1.0 kcal/mol or under -1.0 kcal/mol are shown.

Residue	Number	Interaction type
LEU	83	Hydrogen Bond Pi-Alkyl
GLU	155	Hydrogen Bond
ALA	157	Hydrogen Bond Pi-Alkyl Unfavorable Donor-Donor
GLY	160	Hydrogen Bond
GLU	161	Salt Bridgen Hydrogen Bond
LEU	207	Alkyl

In MK-5108/Aurora A model, the key residues for the binding with MK-5108 are mainly Leu139, Val147, Tyr212, Ala213, Gly216, Thr217, Arg220 and Leu263 with the binding free energy lower than –1 kcal/mol (Fig. 2.14). Arg220 forms the strongest interaction with the ligand (-8.90 kcal/mol) through multiple interactions including hydrogen bond interaction, attractive charge interaction and Pi-Cation interaction. Especially, MK-5108 has a hydrogen bonding interaction with the hydroxyl on the carboxylate group of the ligand and an attractive charge interaction with the carbonyl on the carboxylate group of the ligand, which is the same as LY3295668 (in Fig. 2.15 and Table 8). The residues Lys162, Glu211 and Glu260 contribute unfavorably to the binding of MK-5108 in Aurora A, as indicated by their positive binding free energies. The most unfavorable interaction is generated by Lys162, with the binding free energy of 5.05 kcal/mol.

In MK-5108/Aurora B model, the key residues for the binding with MK-5108 are mainly Val91, Tyr156, Ala157, Gly160, Lys164 and Leu207 with the binding free energy lower than –1 kcal/mol (Fig. 2.16). Lys164 forms the strongest interaction with the ligand (-3.67 kcal/mol). The residues Glu161, Glu204 and Asp218 contribute unfavorably to the binding of MK-5108 in Aurora B, as indicated by their positive binding free energies, with the binding free energy of 2.76 kcal/mol, 1.57 kcal/mol and 1.17 kcal/mol. The ligand-residue interaction types of MK-5108 with Aurora B are listed in Table 9.

In Aurora A, Thr217 and Arg220 show great contributions to the binding with the ligand, with the binding free energy of -5.00 kcal/mol and -9.00 kcal/mol. However, in the binding site of Aurora B, Lys164 (Arg220 in Aurora A) only contributes the binding free energy of -3.67 kcal/mol, Glu161

(Thr217 in Aurora A) even shows a strong unfavorable binding free energy contribution (2.76 kcal/mol). The binding free energy differences of Thr217/Glu161 and Arg220/ Lys164 in Aurora A with Aurora B lead to the difference of selectivity when LY3295668 binds to Aurora kinases. Hence, Thr217 and Arg220 serve as crucial residues of Aurora A when interacting with the ligand MK-5108, rendering MK-5108 a highly selective inhibitor of Aurora A. Additionally, the carboxylate functional group of the inhibitor is pivotal in driving the selectivity differences observed in ligand interactions. This conclusion aligns closely with the findings for LY3295668. It can be inferred that the carboxylate group plays a significant role in the ligand interactions of Aurora A selective inhibitors, particularly in conjunction with the residues Thr217 and Arg220 in Aurora A.

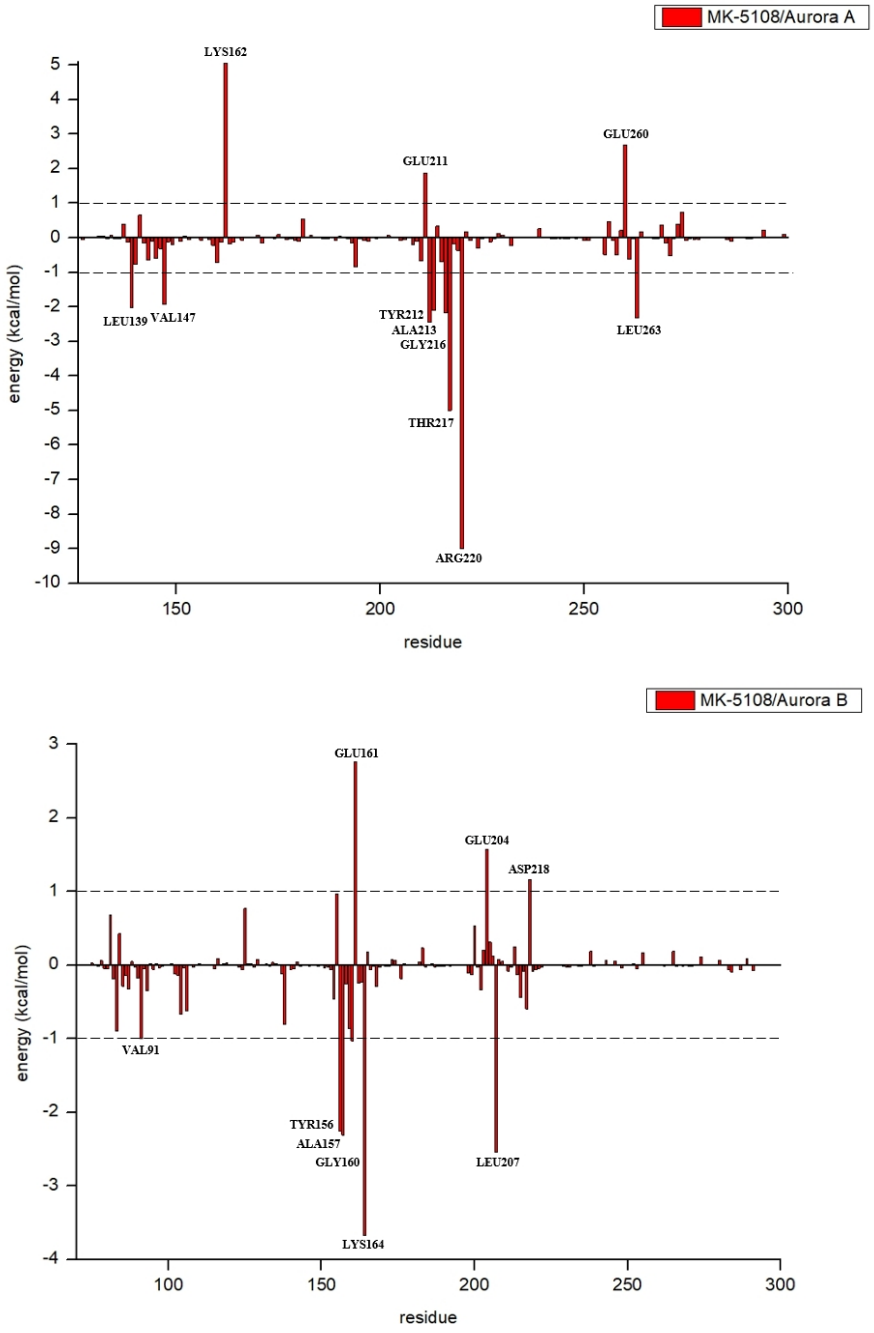

Fig. 2.14 Ligand-residue interaction energies from the MM/PBSA energy decomposition for MK-5108 with Aurora A and B. The residues with energy contributions over 1.0 kcal/mol or under -1.0 kcal/mol are labeled.

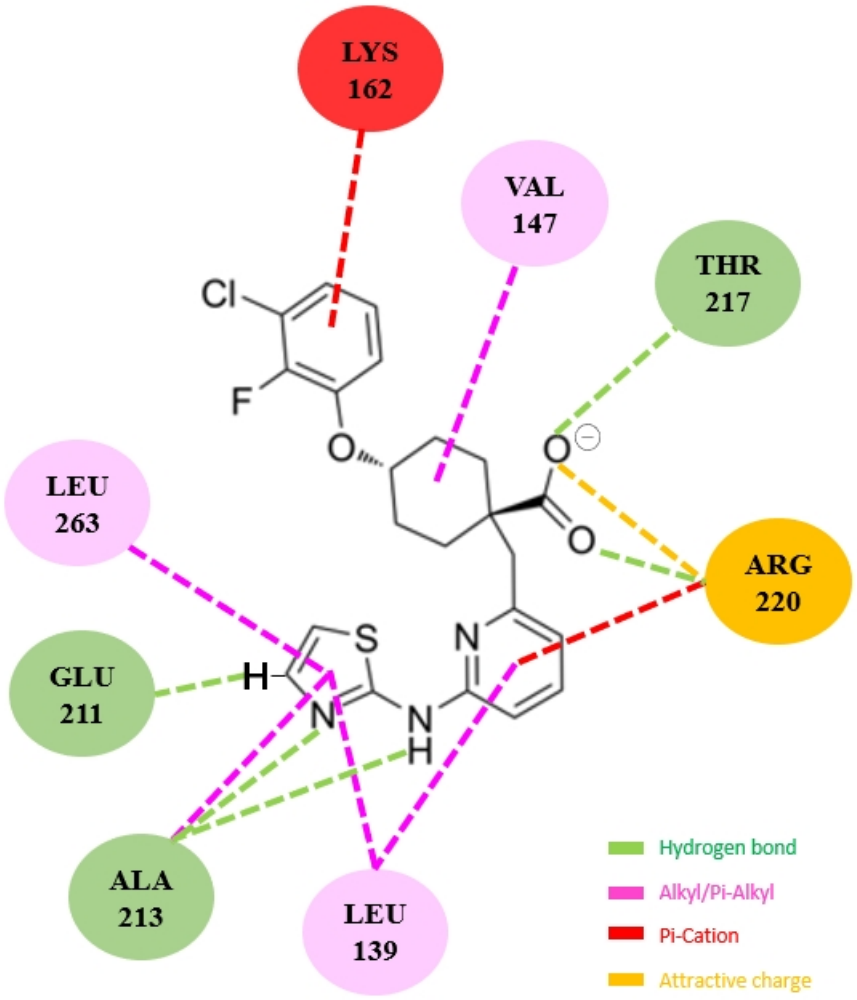

Fig. 2.15 Ligand-residue interactions of MK-5108 with Aurora A. Only the residues with energy contributions over 1.0 kcal/mol or under -1.0 kcal/mol are shown.

Table 8. Ligand-residue interaction types of MK-5108 with Aurora A. Only the residues with energy contributions over 1.0 kcal/mol or under -1.0 kcal/mol are shown.

Residue	Number	Interaction type
LEU	139	Pi-Alkyl
VAL	147	Pi-Alkyl
LYS	162	Pi-Cation
GLU	211	Hydrogen Bond
ALA	213	Hydrogen Bond Pi-Alkyl
THR	217	Hydrogen Bond
ARG	220	Attractive charge Hydrogen Bond Pi-Alkyl
LEU	263	Pi-Alkyl

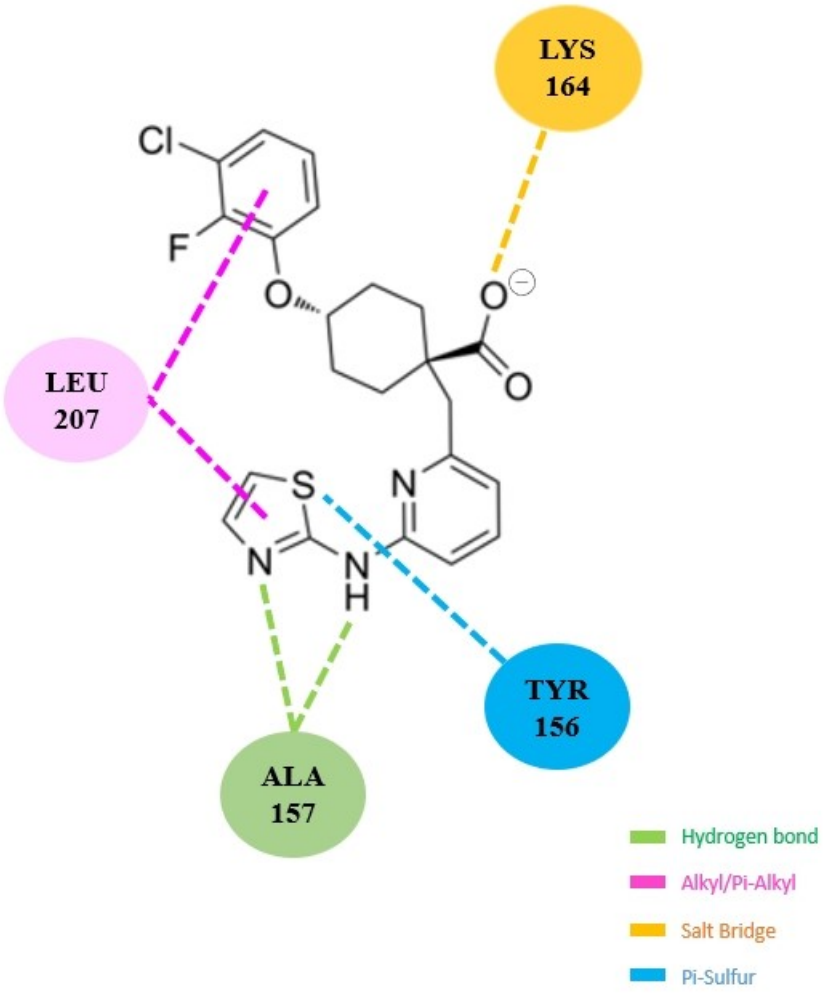

Fig. 2.16 Ligand-residue interactions of MK-5108 with Aurora B. Only the residues with energy contributions over 1.0 kcal/mol or under -1.0 kcal/mol are shown.

Table 9. Ligand-residue interaction types of MK-5108 with Aurora B. Only the residues with energy contributions over 1.0 kcal/mol or under -1.0 kcal/mol are shown.

Residue	Number	Interaction type
TYR	156	Pi-Sulfur
ALA	157	Hydrogen Bond
LYS	164	Salt Bridge
LEU	207	Pi-Alkyl

Per-residue free energy decomposition was applied to the Aurora A and B models to investigate the selectivity mechanism of Alisertib. Residues exhibiting binding free energies lower than –1 kcal/mol are typically regarded as key contributors responsible for ligand binding, as depicted in Fig. 2.17.

In the Alisertib/Aurora A model, the key residues involved in binding with Alisertib include Arg137, Leu139, Val147, Leu194, Leu210, Tyr212, Ala213, and Leu263, all demonstrating binding free energies lower than –1 kcal/mol. Among these, Arg137 exhibits the strongest interaction with the ligand (-4.40 kcal/mol), primarily through a salt bridge interaction with the hydroxyl group on the carboxylate moiety of the ligand (Fig. 2.18). The residues Glu181, Glu211, Glu260 and Asp274 contribute unfavorably to the binding of Alisertib in Aurora A, as indicated by their positive binding free energies. The most unfavorable interaction is generated by Glu260, with the binding free

energy of 1.72 kcal/mol. The ligand-residue interaction types of Alisertib with Aurora A are listed in Table 10.

In Alisertib/Aurora B model, the key residues for the binding with Alisertib are mainly Leu83, Val91, Ala157, Arg159, Leu207 and Ala217 with the binding free energy lower than –1 kcal/mol (Fig. 2.19). Tyr207 forms the strongest interaction with the ligand (-2.27 kcal/mol). The residues Lys106, Glu161, Glu204 and Asp218 contribute unfavorably to the binding of Alisertib in Aurora B, as indicated by their positive binding free energies, with the binding free energy of 2.26 kcal/mol, 2.30 kcal/mol, 1.58 kcal/mol and 1.14 kcal/mol. The ligand-residue interaction types of Alisertib with Aurora B are listed in Table 12, only the residues with energy contributions over 1.0 kcal/mol or under -1.0 kcal/mol are shown.

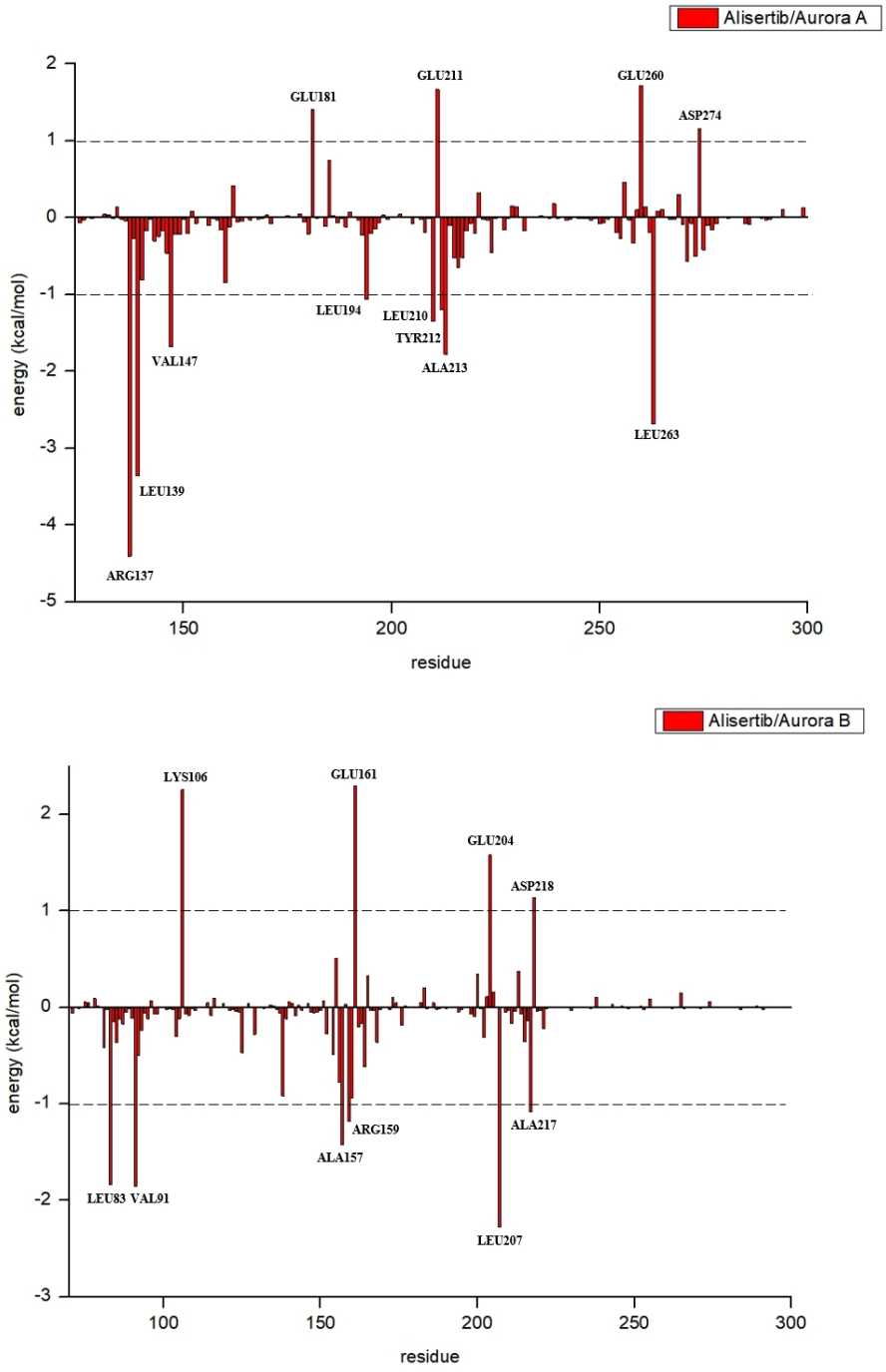

Fig. 2.17 Ligand-residue interaction energies from the MM/PBSA energy decomposition for Alisertib with Aurora A and B. The residues with energy contributions over 1.0 kcal/mol or under -1.0 kcal/mol are labeled.

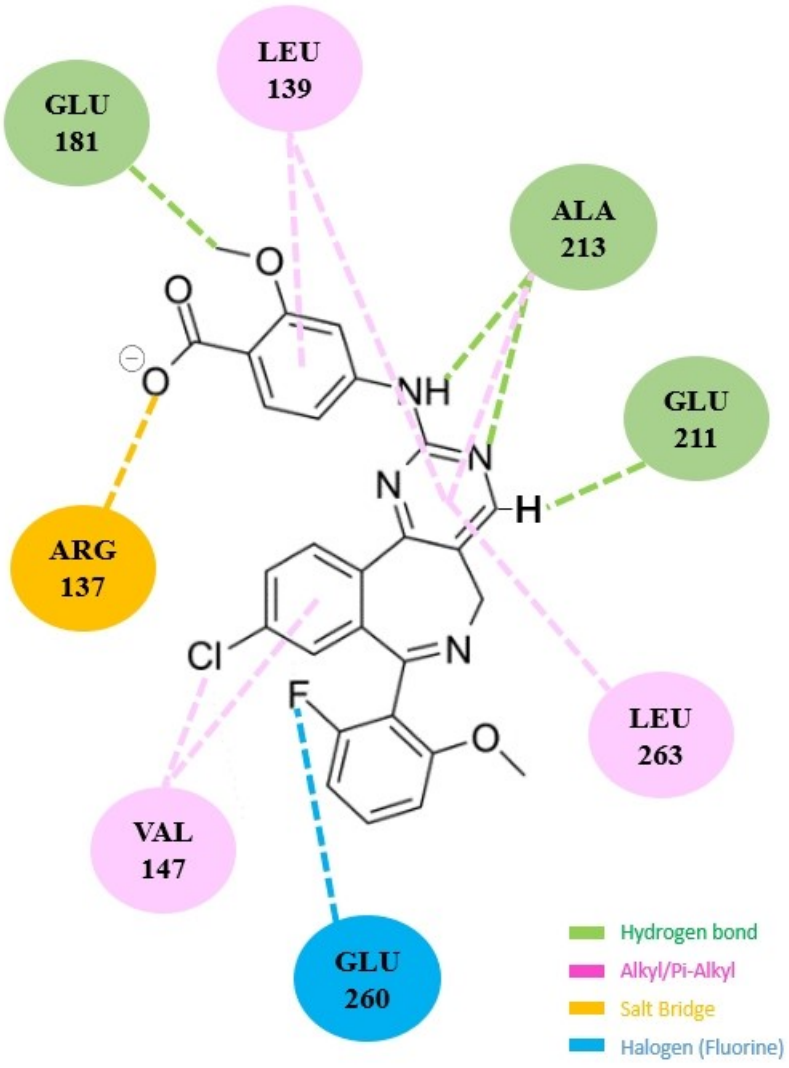

Fig. 2.18 Ligand-residue interactions of Alisertib with Aurora A. Only the residues with energy contributions over 1.0 kcal/mol or under -1.0 kcal/mol are shown.

Table 10. Ligand-residue interaction types of Alisertib with Aurora A. Only the residues with energy contributions over 1.0 kcal/mol or under -1.0 kcal/mol are shown.

Residue	Number	Interaction type
ARG	137	Salt Bridge
LEU	139	Pi-Alkyl
VAL	147	Alkyl Pi-Alkyl
GLU	181	Hydrogen Bond
GLU	211	Hydrogen Bond
ALA	213	Hydrogen Bond Pi-Alkyl
GLU	260	Halogen (Fluorine)
LEU	263	Pi-Alkyl

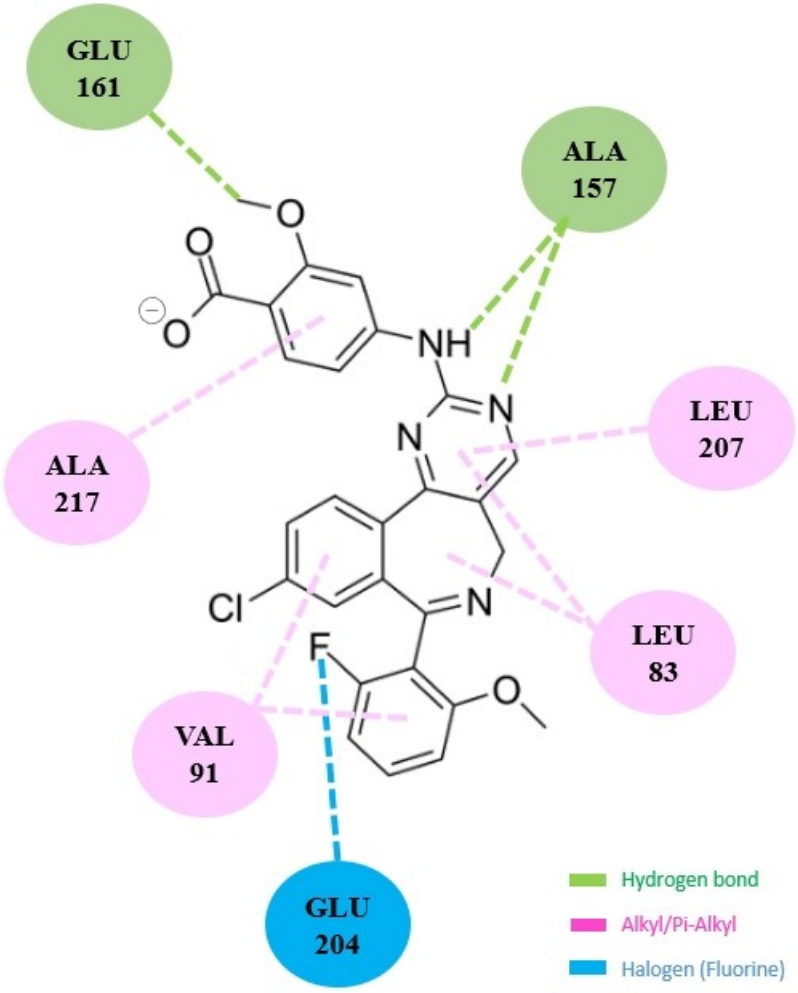

Fig. 2.19 Ligand-residue interactions of Alisertib with Aurora B. Only the residues with energy contributions over 1.0 kcal/mol or under -1.0 kcal/mol are shown.

Table 11. Ligand-residue interaction types of Alisertib with Aurora B. Only the residues with energy contributions over 1.0 kcal/mol or under -1.0 kcal/mol are shown.

Residue	Number	Interaction type
LEU	83	Pi-Alkyl
VAL	91	Pi-Alkyl
ALA	157	Hydrogen Bond
GLU	161	Hydrogen Bond
GLU	204	Halogen (Fluorine)
LEU	207	Pi-Alkyl
ALA	217	Pi-Alkyl

2.8.2 Selectivity Mechanism of Aurora A Selective Ligands

In the ligand-residue interactions of LY3295668, MK-5108, and Alisertib, the carboxylate group in the ligand consistently demonstrates significant contribution. Particularly, it establishes the most significant interaction (-7.99 kcal/mol) between Aurora A and LY3295668 via hydrogen bonding interaction with the hydroxyl of the carboxy group and attractive charge interaction with Arg220 on the carbonyl of the carboxylate group. In MK-5108/Aurora A model, carboxylate shows the strongest interaction (-9.00 kcal/mol) with MK-5108 through hydrogen bond interaction and

attractive charge interaction with Arg220. It also forms the strongest interaction (-4.43 kcal/mol) between Alisertib and the residue Arg137 of Aurora A through salt bridge interaction on the hydroxyl of the carboxylate group. The consistency of the results of LY3295668/Aurora A, MK-5108/Aurora A and Alisertib/Aurora A confirms that the carboxylate group is the key functional group in the binding between Aurora A selective inhibitors and Aurora A, which always contributes the most in the ligand-residue interactions.

In LY3295668/Aurora A model and MK-5108/Aurora A model, Thr217 and Arg220 both are located in the hinge region of Aurora kinase and show the greatest contributions to the binding with the ligand, while they are not markedly correlated with the ligand in Alisertib/Aurora A model. However, Glu161 (Thr217 in Aurora A) shows a strong unfavorable binding free energy contribution (2.230 kcal/mol) in Alisertib/Aurora B model, which has a difference of 2.818kcal/mol with the binding free energy contribution of Thr217 in Aurora A. Glu161 (Thr217 in Aurora A) also contributes unfavorably to the binding of LY3295668 and MK-5108 in Aurora B with positive binding free energies.

It is evident that Thr217 and Arg220/137 in Aurora A emerge as the most crucial key residues in binding with Aurora kinase inhibitors, thereby contributing significantly to the discernible difference in subtype selectivity between Aurora A and B.

The key residues, along with their binding free energy contributions, types, and locations of Aurora A and B binding with LY3295668, MK-5108, and Alisertib, are listed in Table 12 and Table 13, respectively.

Table 12. Key residues with the binding free energy contributions, types and locations of Aurora A binding with LY3295668, MK-5108 and Alisertib.

	LY3295668		MK-5108		Alisertib		
Residue	Type	Energy kcal/mol	Type	Energy kcal/mol	Type	Energy kcal/mol	Position
ARG 137	HB	1.29	/	0.40	SB	-4.40	Glycine rich loop
LEU 139	/	-1.33	PAl	-2.03	PAl	-3.36	Glycine rich loop
VAL 147	/	-0.73	PAl	-1.93	Al, PAl	-1.68	Glycine rich loop
LYS 162	Al, HB	4.95	PC	5.05	/	0.42	N-lobe
GLU 181	/	-0.17	/	0.54	HB	1.40	αC helix
GLU 211	HB	-1.47	HB	1.88	HB	1.67	Hinge region (active site)
ALA 213	HB, Al, UDD	-1.81	HB, PAl	-2.11	HB, PAl	-1.78	Hinge region (active site)
GLY 216	HB	-2.31	/	-2.17	/	-0.65	Hinge region (active site)
THR 217	HB	-2.44	HB	-5.00	/	-0.52	Hinge region (active site)
ARG 220	AC, HB	-7.99	AC, HB, PC	-9.00	/	-0.20	Hinge region (active site)
GLU 260	/	1.64	/	2.69	Ha	1.72	Activation loop
LEU 263	Al	-2.28	PAl	-2.33	PAl	-2.68	Activation loop
ALA 273	Ha, Al	1.27	/	0.40	/	/	Activation loop

HB=Hydrogen bond, Al=Alkyl, PAl=Pi-Alkyl, UDD=Unfavourable Donor-Donor, AC=Attractive Charge, Ha=Halogen, PC=Pi-Cation, SB=Salt Bridge

Table 13. Key residues with the binding free energy contributions , types and locations of Aurora B binding with LY3295668, MK-5108 and Alisertib.

	LY3295668		MK-5108		Alisertib		
Residue	Type	Energy kcal/mol	Type	Energy kcal/mol	Type	Energy kcal/mol	Position
LEU 83	HB, PAl	-1.48	/	-0.90	PAl	-1.84	Glycine rich loop
VAL 91	/	-0.81	/	-1.00	PAl	-1.85	Glycine rich loop
GLU 155	HB	-1.15	/	0.97	/	0.51	Hinge region (active site)
TYR 156	/	-2.54	PS	-2.26	/	-0.78	Hinge region (active site)
ALA 157	HB, PAl, UDD	-1.96	HB	-2.31	HB	-1.42	Hinge region (active site)
GLY 160	HB	-2.07	/	-1.03	/	-0.94	Hinge region (active site)
GLU 161	SB, HB	4.48	/	2.76	HB	2.30	Hinge region (active site)
LYS 164	/	-1.98	SB	-3.67	/	-0.62	Hinge region (active site)
GLU 204	/	4.89	/	1.57	Ha	1.58	Activation loop
LEU 207	Al	-2.36	PAl	-2.54	PAl	-2.27	Activation loop
ALA 217	/	-0.13	/	-0.59	PAl	-1.08	Activation loop

HB=Hydrogen bond, Al=Alkyl, PAl=Pi-Alkyl, UDD=Unfavourable Donor-Donor, AC=Attractive Charge, Ha=Halogen, PC=Pi-Cation, SB=Salt Bridge, PS=Pi-Sulfur

CHAPTER THREE

EVALUATION OF AURORA B SELECTIVE INHIBITORS BINDING WITH AURORA KINASE A AND B BY MOLECULAR DYNAMICS SIMULATION.

3.1 GSK-1070916

Build the systems

Due to the lack of complex crystal structures and ligand structure, molecular docking was performed to build the structures of Aurora A and B bound with the ligand GSK-1070916. Specifically, the structure of GSK-1070916 was drawn by Chemdraw, Aurora A and B structures were retrieved from AlphaFold Protein Structure Database: Homo sapiens Aurora kinase A and B, the AlphaFold database access ID are AF-A3KFJ2-F1 and AF-A0A3D4H337-F1. The program Autodock Vina including four steps: building the systems, docking calculation, scoring, and finding the best conformation could give the best binding conformation predicted to achieve this goal, which is much faster and more accurate depending on the system. Significantly, the net charge of GSK-1070916 was set to 1 when preparing the systems due to its protonation state at the pH of 7.4. The starting structures of Aurora kinase A and B binding with GSK-1070916 by molecular docking are shown in Fig. 3.1.

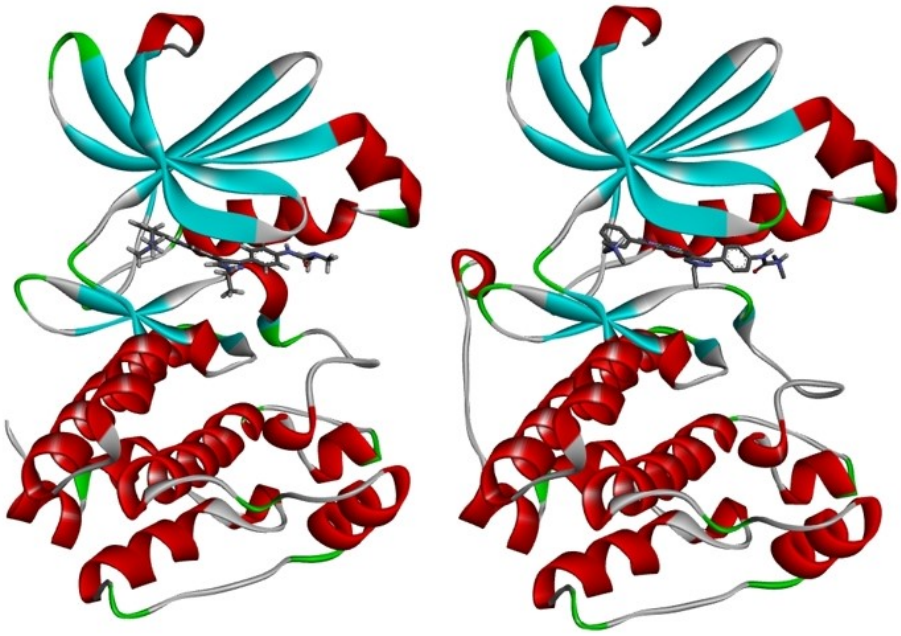

Fig. 3.1 Starting structures of Aurora kinase A and B binding with GSK-1070916.

Stability of complex models and ligand interactions

Root-mean-square deviations (RMSD) of GSK-1070916 binding with Aurora A and B from the starting structures were analyzed to explore the dynamic stability of complexes and ensure the rationality of the sampling method during the 50ns MD simulation for each complex (Fig. 3.2). The figures shows the proteins and ligands in two systems were stable after equilibrium.

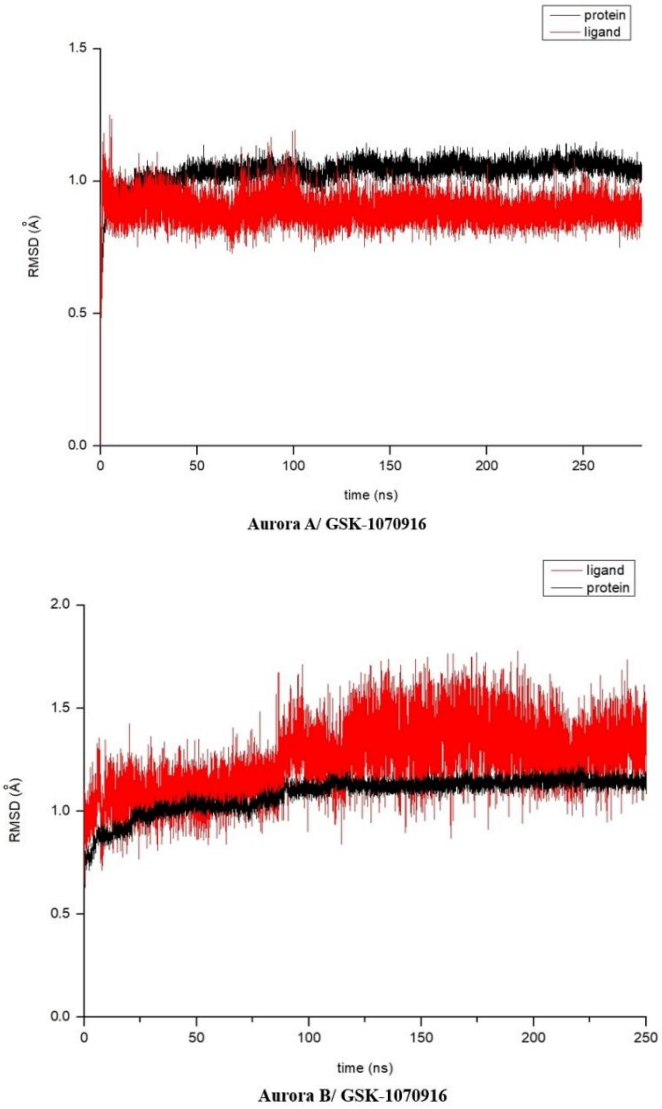

Fig. 3.2 The root mean square deviation (RMSD) of Aurora kinase A and B binding with GSK-1070916.

According to the average structure and ligand interactions of GSK-1070916 binding with Aurora A and B, GSK-1070916 was stabilized in the binding pocket formed by residues Leu139, Lys143, Phe144, Val147, Leu164, Arg220, Glu260, Leu263, Ala273 and Asp274 for Aurora A; Arg81, Leu83, Lys85, Gly86, Lys87, Phe88, Val91, Ala104, Tyr156, Ala157, Arg159, Glu161, Leu207,

Ala217, Asp218 and Trp221 for Aurora B (Fig. 3.3).

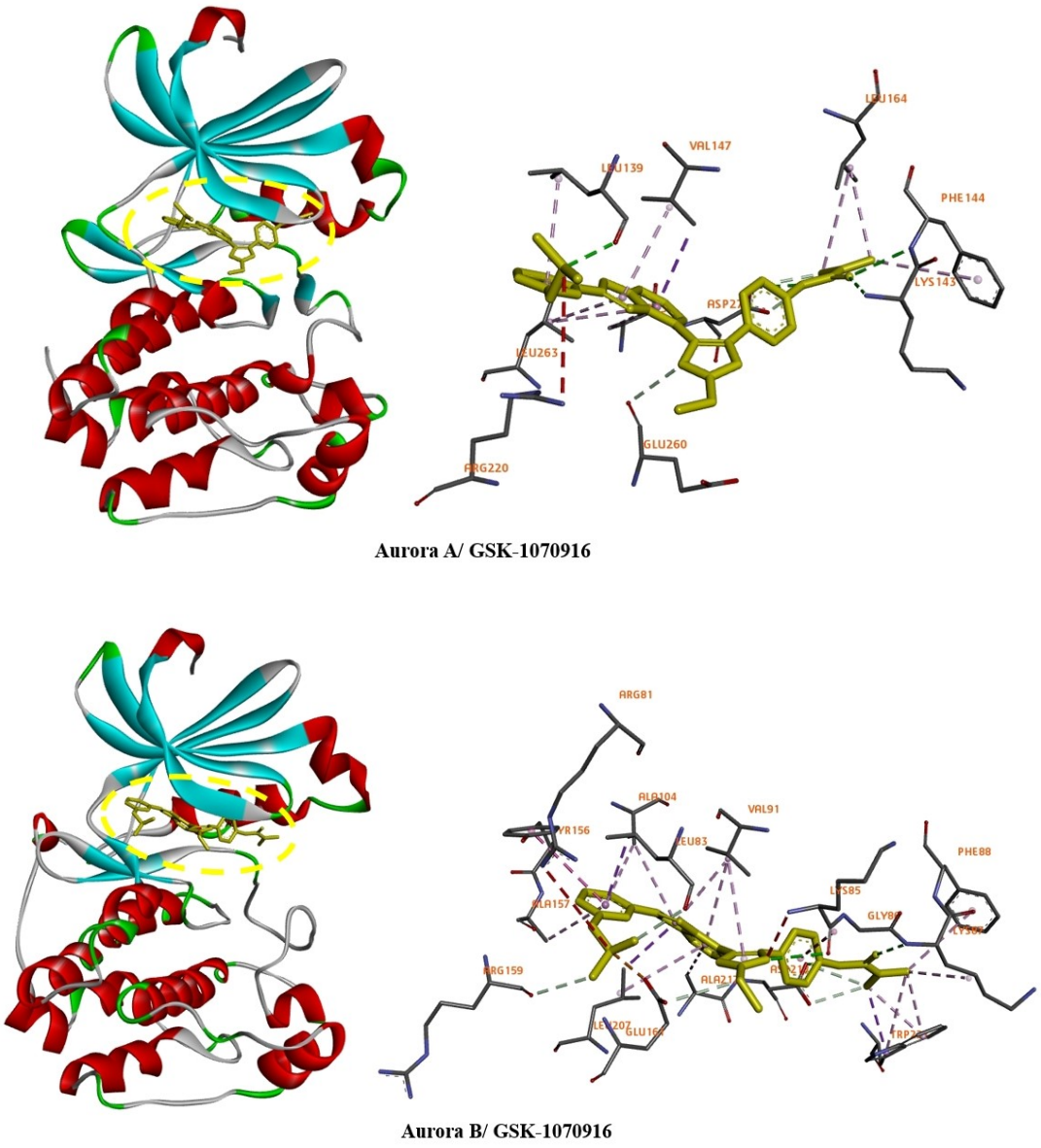

Fig. 3.3 Average structures and ligand interactions of Aurora kinase A and B binding with GSK-1070916.

Binding free energy calculations

In Table 14, the binding free energies of the Aurora A/GSK-1070916 model and the Aurora B/GSK-1070916 model were calculated using the MM/PBSA method. It can be observed that the energy ranking predicted by the MM/PBSA method is reasonable compared to the data of IC_{50}. GSK-1070916 exhibits a more favorable binding with Aurora B, indicating its potential as an Aurora B selective inhibitor.

Table 14. The binding free energy of Aurora A and B with GSK-1070916 calculated from MM/PBSA method and IC_{50}.

System	ΔG_{PB} (kcal/mol)	IC_{50} (nM)
Aurora A/GSK-1070916	-23.07	＞100
Aurora B/GSK-1070916	-36.37	0.38

Mechanisms of selectivity for GSK-1070916 over Aurora kinase A and B

Residues with binding free energy lower than –1 kcal/mol are generally considered as key contributors responsible for ligand binding. As shown in Fig. 3.4, in GSK-1070916/ Aurora A model, the key residues for the binding with GSK-1070916 are mainly Leu139, Gly142, Lys143, Phe144, Val147 and Leu263 with the binding free energy lower than –1 kcal/mol. Leu139 forms

the strongest interaction (-2.80 kcal/mol) through hydrogen bonding interaction with the methyl group on tertiary amine side chain of the ligand, and Pi-Alkyl interaction with the ligand (Fig. 3.5 and Table 15). The residues Glu181, Arg220 and Glu260 contribute unfavorably to the binding of GSK-1070916 in Aurora A, as indicated by their positive binding free energies. The most unfavorable interaction is generated by Glu260, with the binding free energy of 2.48 kcal/mol.

In GSK-1070916/ Aurora B model, the key residues for the binding with GSK-1070916 are Gly86, Lys87, Phe88, Val91, Glu125, Arg159, Gly160, Leu207, Asp218 and Trp221 with the binding free energy lower than –1 kcal/mol. Asp218 forms the strongest interaction (-2.18 kcal/mol) through hydrogen bonding interaction with the methyl group on tertiary amine side chain of the ligand. The residues Arg81, Lys106, Glu121, Ala157 and Lys168 contribute unfavorably to the binding of GSK-1070916 in Aurora B, as indicated by their positive binding free energies, with the binding free energy of 2.31 kcal/mol, 1.34 kcal/mol, 1.17 kcal/mol, 1.55 kcal/mol and 1.11 kcal/mol, respectively (Fig. 3.6 and Table 16).

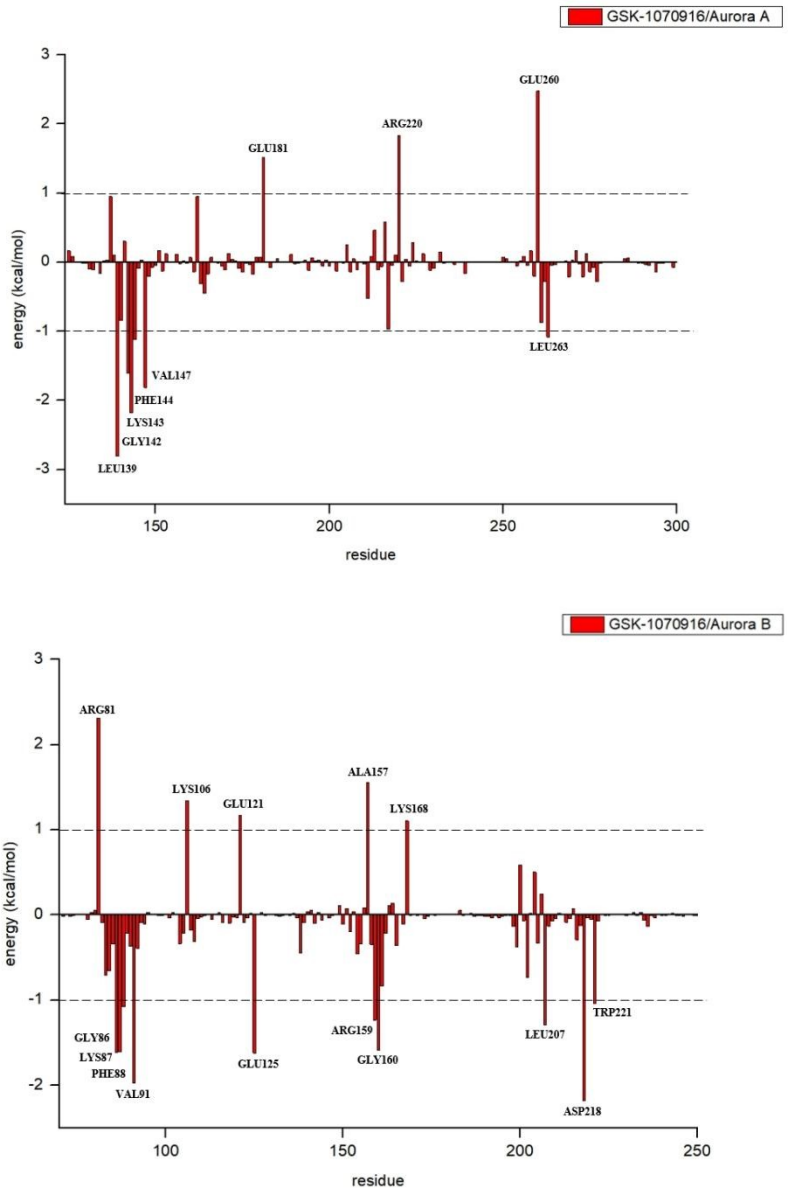

Fig. 3.4 Ligand-residue interaction energies from the MM/PBSA energy decomposition for GSK-1070916 with Aurora A and B. The residues with energy contributions over 1.0 kcal/mol or under -1.0 kcal/mol are labeled.

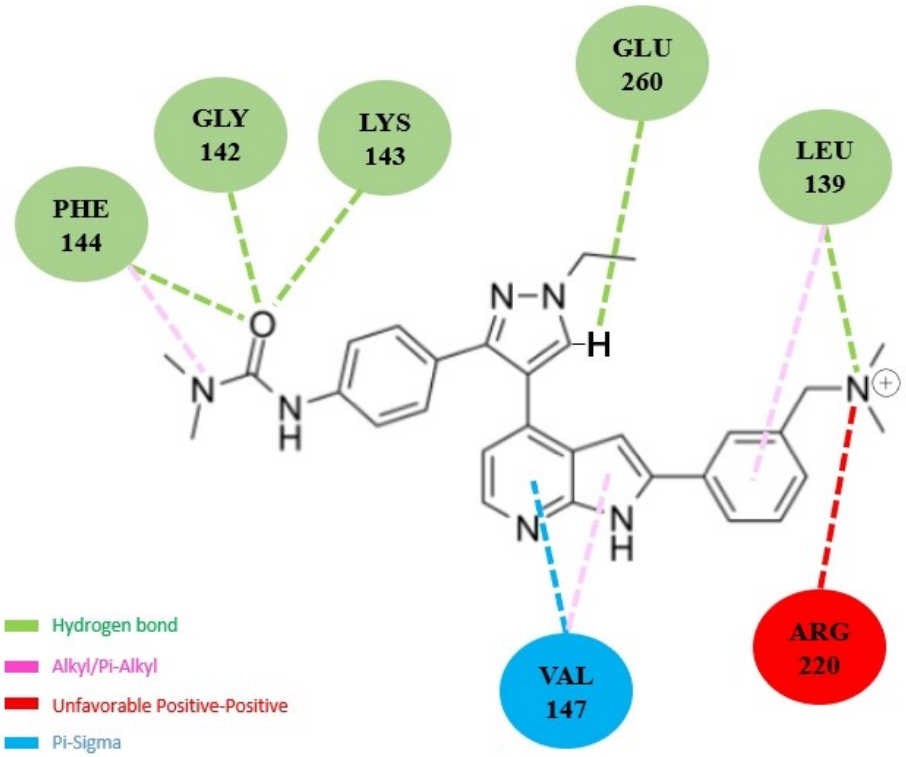

Fig. 3.5 Ligand-residue interactions of GSK-1070916 with Aurora A. Only the residues with energy contributions over 1.0 kcal/mol or under -1.0 kcal/mol are shown.

Table 15. Ligand-residue interaction types of GSK-1070916 with Aurora A. Only the residues with energy contributions over 1.0 kcal/mol or under -1.0 kcal/mol are shown.

Residue	Number	Interaction type	Energy contribution (kcal/mol)	Location
LEU	139	Hydrogen Bond Pi-Alkyl	-2.80	Glycine rich loop
GLY	142	Hydrogen Bond	-1.60	Glycine rich loop
LYS	143	Hydrogen Bond	-2.18	Glycine rich loop
PHE	144	Hydrogen Bond Alkyl	-1.12	Glycine rich loop
VAL	147	Pi-Sigma Pi-Alkyl	-1.81	Glycine rich loop
ARG	220	Unfavorable Positive-Positive	1.84	Hinge region (active site)
GLU	260	Hydrogen Bond	2.48	Activation loop

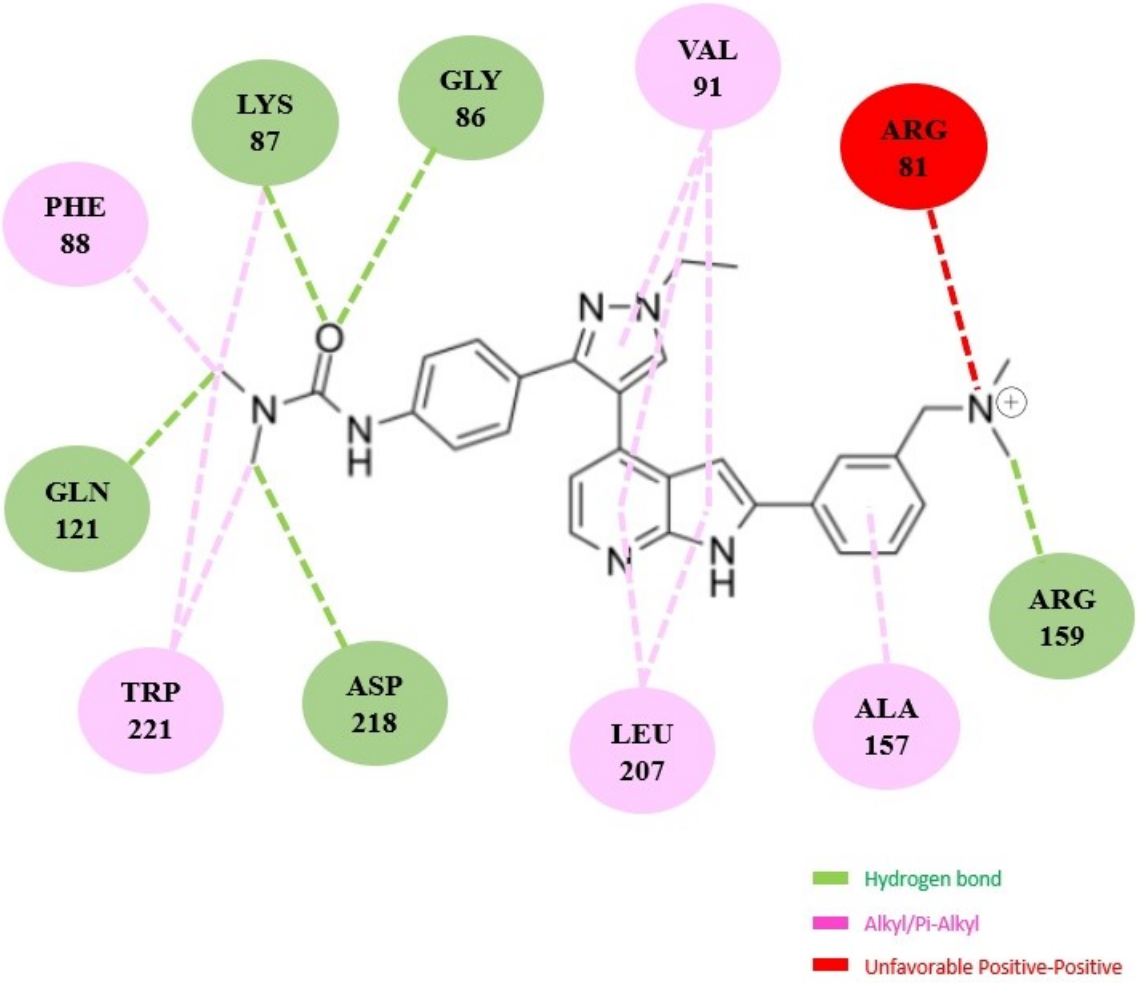

Fig. 3.6 Ligand-residue interactions of GSK-1070916 with Aurora B. Only the residues with energy contributions over 1.0 kcal/mol or under -1.0 kcal/mol are shown.

Table 16. Ligand-residue interaction types of GSK-1070916 with Aurora B. Only the residues with energy contributions over 1.0 kcal/mol or under -1.0 kcal/mol are shown.

Residue	Number	Interaction type	Energy contribution (kcal/mol)	Location
ARG	81	Unfavorable Positive-Positive	2.31	Glycine rich loop
GLY	86	Hydrogen Bond	-1.61	Glycine rich loop
LYS	87	Hydrogen Bond Alkyl	-1.61	Glycine rich loop
PHE	88	Alkyl	-1.08	Glycine rich loop
VAL	91	Pi-Alkyl	-1.97	Glycine rich loop
GLN	121	Hydrogen Bond	1.17	αC helix
ALA	157	Pi-Alkyl	1.55	Hinge region (active site)
ARG	159	Hydrogen Bond	-1.23	Hinge region (active site)
LEU	207	Pi-Alkyl	-1.29	Activation loop
ASP	218	Hydrogen Bond	-2.18	Activation loop
TRP	221	Alkyl	-1.04	Activation loop

3.2 Contrasting Selectivity Mechanisms in Aurora B and Aurora A Ligands

As mentioned previously, there are only four residues around the binding site that differ between Aurora A and B, located near the ATP-binding pocket in the solvent-exposed region. These residues are Leu215, Thr217, Val218, and Arg220 in Aurora A, while the corresponding residues in Aurora B are Arg159, Glu161, Leu162, and Lys164. Numerous studies suggest that targeting these residues in the active site can modulate the selectivity of inhibitors towards either Aurora A or Aurora B. As shown in Table 15 and Table 16, the energy contributions from the residues are Leu215 (0.06 kcal/mol), Thr217 (-0.97 kcal/mol), Val218 (-0.05 kcal/mol), Arg220 (1.84 kcal/mol) in the Aurora A active model and Arg159 (-1.23 kcal/mol), Glu161 (-1.59 kcal/mol), Leu162 (-0.21 kcal/mol), Lys164 (0.14 kcal/mol) correspondingly in the Aurora B active model. The differences are -1.30 kcal/mol, -0.62 kcal/mol, -0.17 kcal/mol and 1.70kcal/mol, respectively. The most significant binding free energy difference between the Aurora A residue Leu215 (0.06 kcal/mol) and the Aurora B residue Arg159 (-1.23 kcal/mol) suggests that the key residue contributing to the ligand selectivity is Arg159 in Aurora B, which anchors the ligand to the ATP-binding pocket. As shown in Fig. 3.6, Arg159 forms the interaction through a weak hydrogen bond with the methyl group on tertiary amine side chain at the end of the ligand. Moreover, according to the energy decomposition of Arg159, it shows the strong polar solvation interaction of Arg159 make it favorable to the binding. Additionally, Asp218 forms the strongest interaction (-2.18 kcal/mol) through hydrogen bonding interaction with the methyl group on tertiary amine side chain at other end of the ligand. It can be predicted that the tertiary amine with a methyl group is the key functional group of the

Aurora B selective inhibitor when binding to Aurora B.

According to the results of LY3295668, MK-5108 and Alisertib, Thr217 and Arg220/137 are the most significant key residues with an evident difference in the binding free energy contribution when binding with Aurora A and B, which leads to the high selectivity for Aurora A over B. The results of Aurora B selective inhibitor GSK-1070916 shows that the binding free energy of Thr217, Arg220 and Arg137 in the Aurora A model are insignificant, which agrees with the previous conclusion about selectivity in this research.

CHAPTER FOUR

EVALUATION OF AURORA PAN-INHIBITORS BINDING WITH AURORA KINASE A AND B BY MOLECULAR DYNAMICS SIMULATION.

4.1 Danusertib

Build the systems

The Danusertib/Aurora A model and Danusertib/Aurora B model were constructed by structurally superimposing the crystal Aurora A (3E5A) and the AlphaFold structure of Aurora B (AF-A0A3D4H337-F1) to the crystal complex of Aurora A/Danusertib (PDB ID: 2J50) as shown in Fig. 4.1. Significantly, the net charge of Danusertib was set to 2 when preparing the systems due to its protonation state at the pH of 7.4.

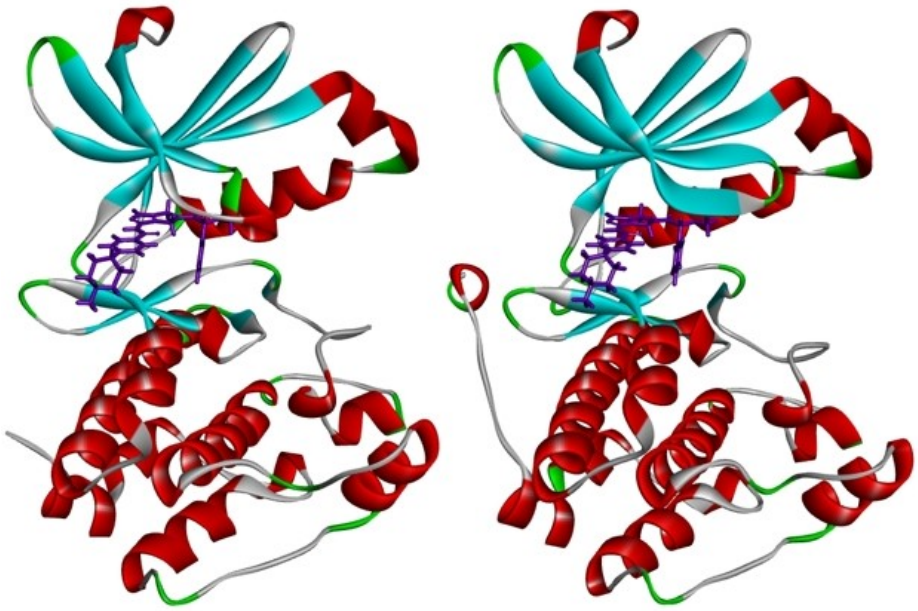

Fig. 4.1 Starting structures of Aurora kinase A and B binding with Danusertib.

Stability of complex models and ligand interactions

The RMSDs of Danusertib binding with Aurora A and B were analyzed to explore the dynamic stability of complexes and ensure the rationality of the sampling method during the 50ns MD simulation for each complex (Fig. 4.2). The figures show that the proteins and ligands in both systems were stable after equilibrium.

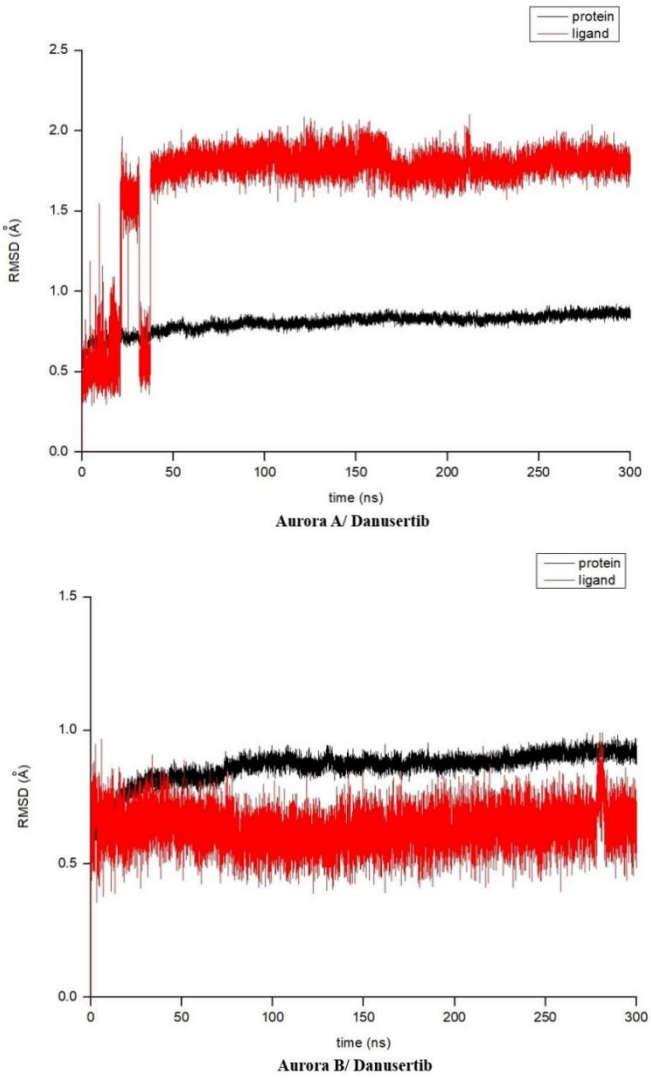

Fig. 4.2 The root mean square deviation (RMSD) of Aurora kinase A and B binding with Danusertib.

The average structures and ligand interactions shown in Fig. 4.3 claims that GSK-1070916 was stabilized in the binding pocket formed by residues Leu139, Lys143, Phe144, Ala160, Lys162, Glu211, Ala213, Pro214, Leu215, Gly216, Leu263 and Asp274 for Aurora A; Arg81, Leu83, Val91, Ala104, Lys106, Leu138, Glu155, Ala157, Pro158, Arg159, Glu161, Glu165, Leu207 and Ala217 for Aurora B.

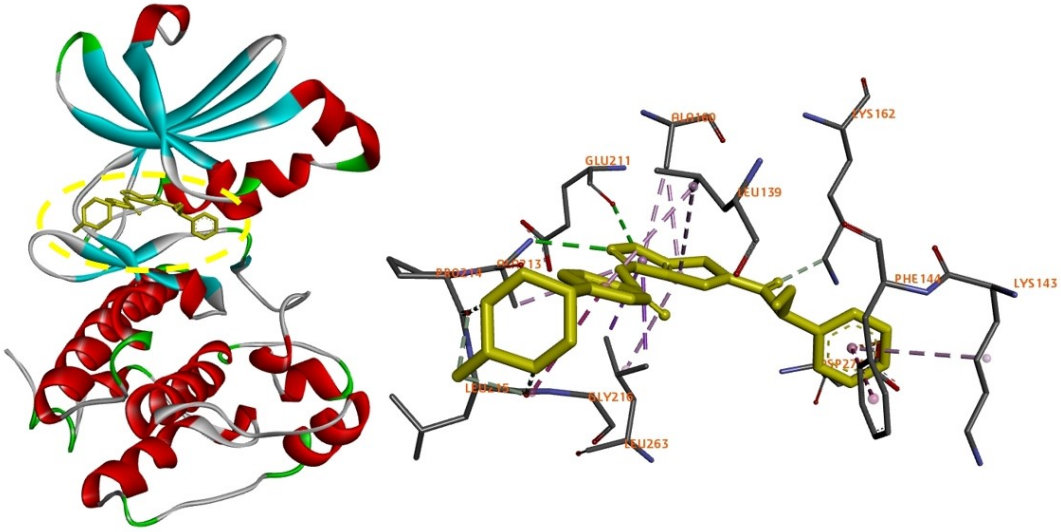

Aurora A/ Danusertib

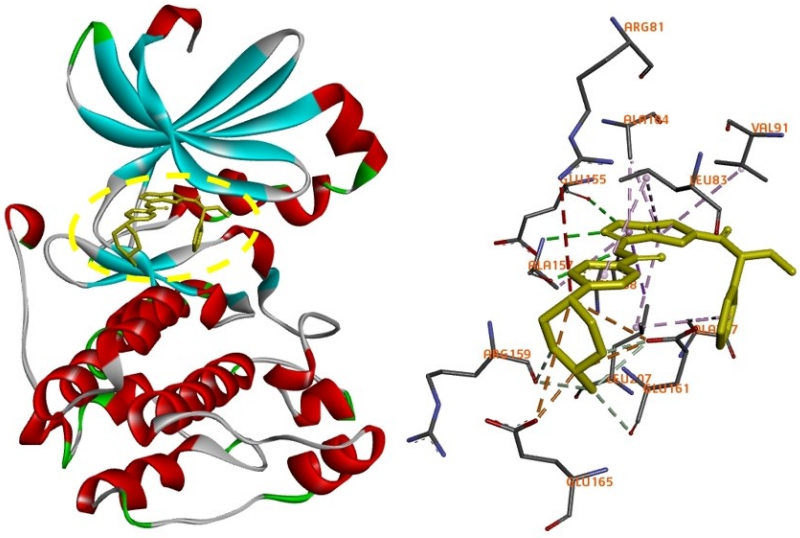

Aurora B/ Danusertib

Fig. 4.3 Average structures and ligand interactions of Aurora kinase A and B binding with Danusertib.

Binding free energy calculations

In Table 17, the binding free energies of the Aurora A/Danusertib model and the Aurora B/Danusertib model were calculated using the MM/PBSA method. It can be observed that the binding free energies predicted by the MM/PBSA method are consistent with the reported IC_{50} data.

Table 17. The binding free energy of Aurora A and B with Danusertib calculated from MM/PBSA method and IC_{50}.

System	ΔG_{PB} (kcal/mol)	IC_{50} (nM)
Aurora A/Danusertib	-32.75	13
Aurora B/Danusertib	-34.01	79

Mechanisms of selectivity for Danusertib over Aurora kinase A and B

In the Danusertib/Aurora A model, the key residues involved in binding with Danusertib include Leu139, Phe144, Val147, Lys162, Glu211, Tyr212, Ala213, Thr217, and Leu263, with binding free energies lower than –1 kcal/mol. Among these, Glu211 forms the strongest interaction with the ligand (-4.17 kcal/mol) through a hydrogen bond (Fig. 4.4). Additionally, residues Lys143, Lys224, and Asp274 contribute unfavorably to the binding of Danusertib in Aurora A, as indicated by their positive binding free energies. Notably, the most unfavorable interaction is generated by Lys143, with a binding free energy of 1.28 kcal/mol. The types of ligand-residue interactions, energies, and locations for the Danusertib/Aurora A model are listed in Table 17. In the Alisertib/Aurora B model, the key residues involved in binding with Alisertib include Leu83, Val91, Glu155, Tyr156, Ala157, Pro158, and Leu207, with binding free energies lower than –1 kcal/mol. Among these, Glu155 forms the strongest interaction with the ligand (-5.08 kcal/mol). Additionally, residues Arg81, Glu161, and Asp218 contribute unfavorably to the binding of Alisertib in Aurora B, as indicated by their positive binding free energies, which are 1.30 kcal/mol, 2.95 kcal/mol, and 2.78 kcal/mol, respectively.

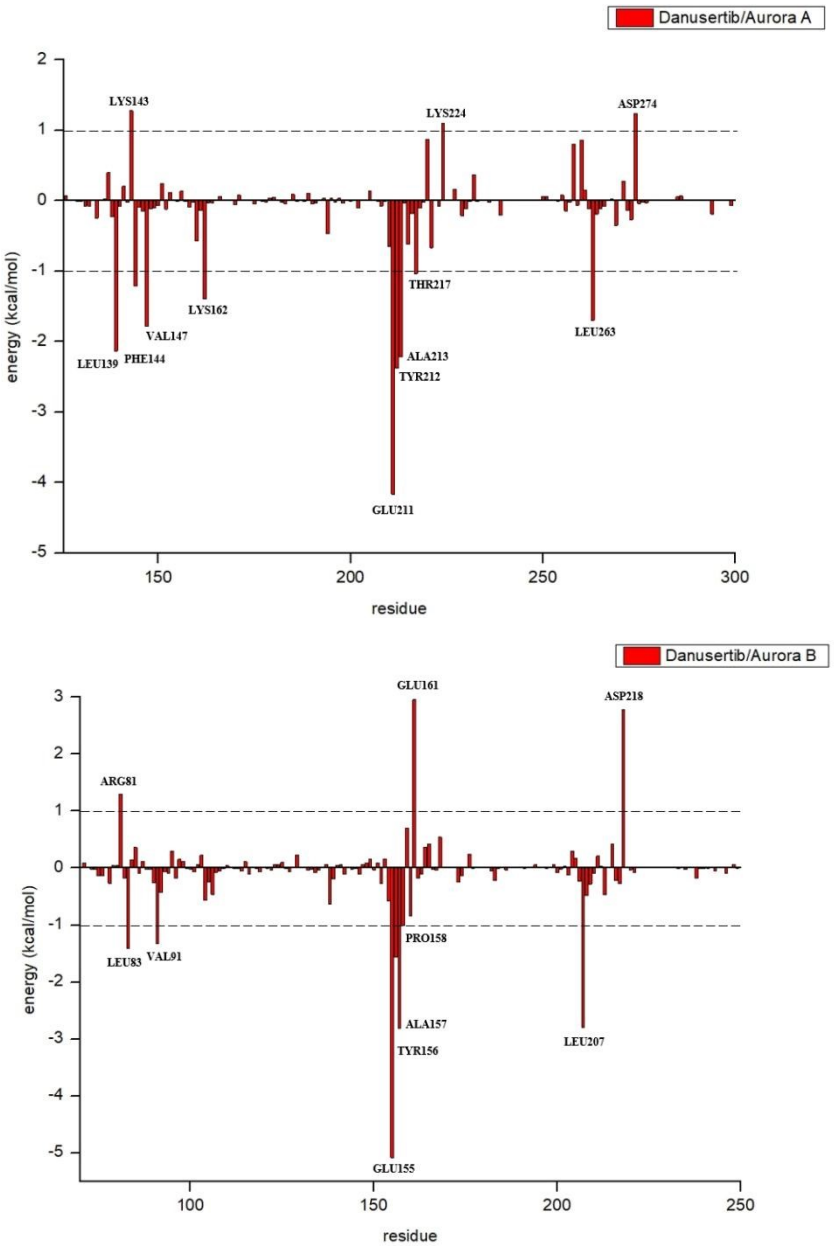

Fig. 4.4 Ligand-residue interaction energies from the MM/PBSA energy decomposition for Danusertib with Aurora A and B. The residues with energy contributions over 1.0 kcal/mol or under -1.0 kcal/mol are labeled.

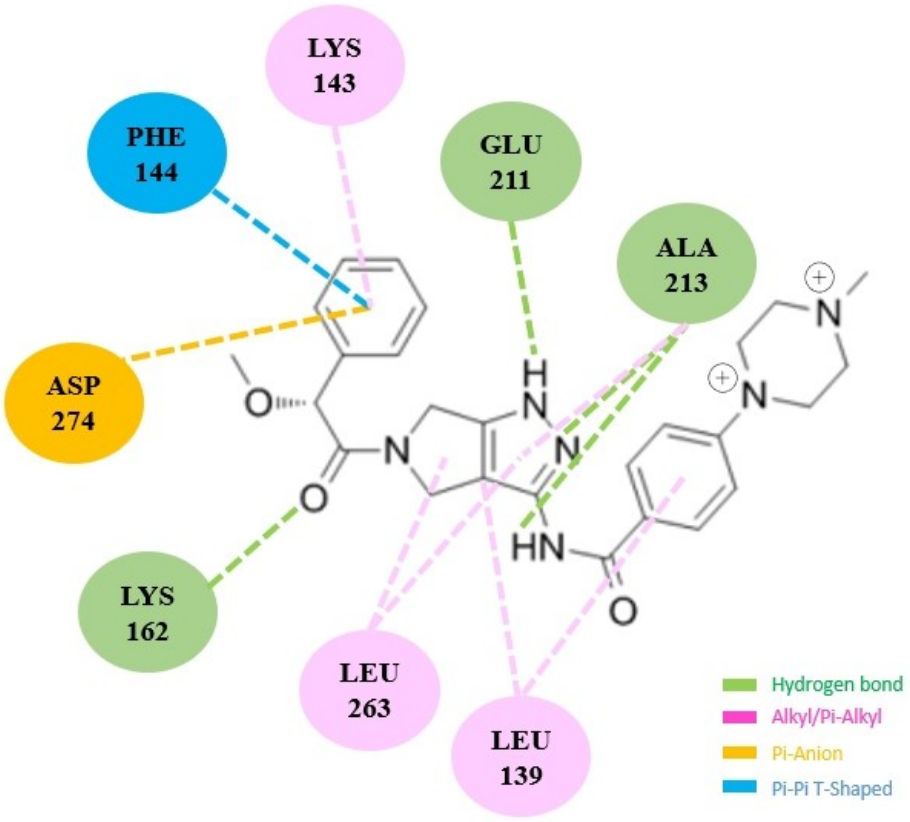

Fig. 4.5 Ligand-residue interactions of Danusertib with Aurora A. Only the residues with energy contributions over 1.0 kcal/mol or under -1.0 kcal/mol are shown.

Table 17. Ligand-residue interaction types of Danusertib with Aurora A. Only the residues with energy contributions over 1.0 kcal/mol or under -1.0 kcal/mol are shown.

Residue	Number	Interaction type	Energy contribution (kcal/mol)	Location
LEU	139	Alkyl Pi-Alkyl	-2.13	Glycine rich loop
LYS	143	Pi-Alkyl	1.28	Glycine rich loop
PHE	144	Pi-Pi T-Shaped	-1.21	Glycine rich loop
LYS	162	Hydrogen Bond	-1.40	N-lobe
GLU	211	Hydrogen Bond	-4.17	Hinge region (active site)
ALA	213	Hydrogen Bond Alkyl	-2.21	Hinge region (active site)
LEU	263	Alkyl	-0.82	Activation loop
ASP	274	Pi-Anion	1.24	Activation loop

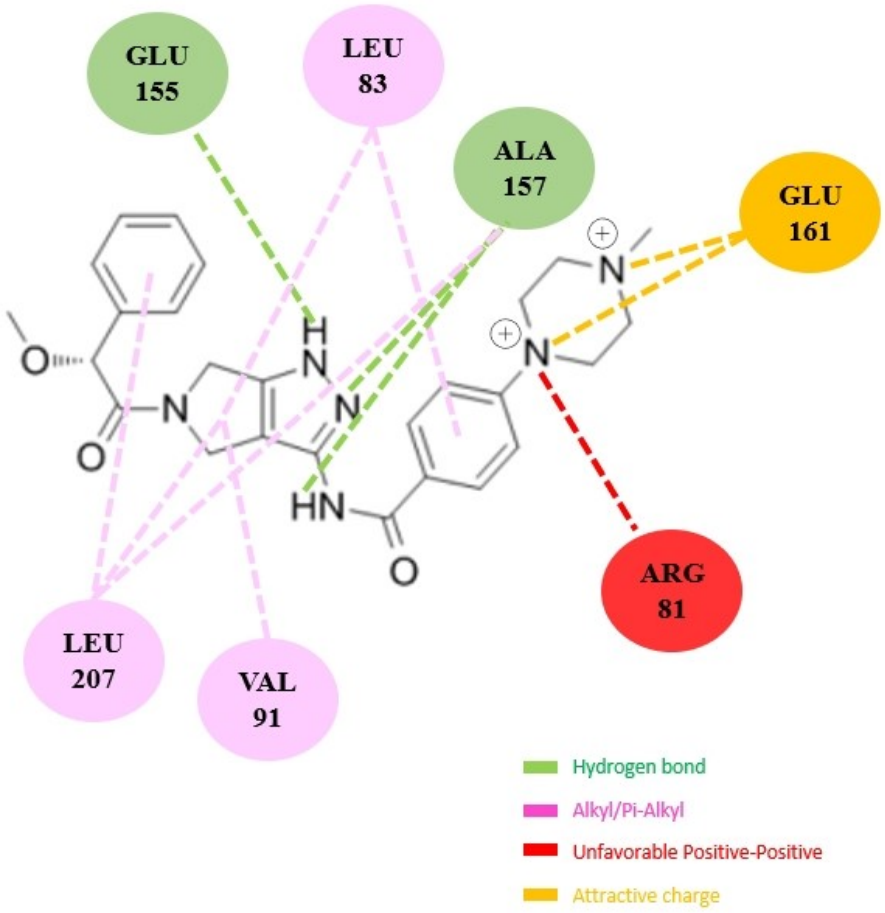

Fig. 4.6 Ligand-residue interactions of Danusertib with Aurora B. Only the residues with energy contributions over 1.0 kcal/mol or under -1.0 kcal/mol are shown.

Table 18. Ligand-residue interaction types of Danusertib with Aurora B. Only the residues with energy contributions over 1.0 kcal/mol or under -1.0 kcal/mol are shown.

Residue	Number	Interaction type	Energy contribution (kcal/mol)	Location
ARG	81	Unfavorable Positive-Positive	1.30	Glycine rich loop
LEU	83	Hydrogen Bond	-1.41	Glycine rich loop
VAL	91	Hydrogen Bond Alkyl	-1.33	Glycine rich loop
GLU	155	Alkyl	-5.08	Hinge region (active site)
ALA	157	Pi-Alkyl	-2.81	Hinge region (active site)
PRO	158	Hydrogen Bond	-1.00	Hinge region (active site)
GLU	161	Pi-Alkyl	2.95	Hinge region (active site)
LEU	207	Hydrogen Bond	-2.79	Activation loop

4.2 Contrasting Selectivity Mechanisms in Pan-inhibitor with Aurora A and B Ligands

According to the results obtained for LY3295668, MK-5108, and Alisertib, Thr217 and Arg220/137 emerge as the most significant key residues, displaying a notable difference in binding free energy contribution when interacting with Aurora A and B. This discrepancy contributes to the high selectivity of these inhibitors for Aurora A over Aurora B.

In contrast, Arg220 and Arg137 both show unfavourable contributions to the binding with Aurora A obviously. The findings concerning the Aurora B selective inhibitor Danusertib indicate that the binding free energy of Thr217 (-1.033 kcal/mol) in the Aurora A model is not sufficiently influential, and Danusertib does not exhibit direct interactions with Thr217. Furthermore, it's notable that Danusertib lacks a carboxylate group, which has been established as a key functional group for Aurora A selective inhibitors binding to Aurora A. Consequently, Danusertib demonstrates only a slightly favorable trend in binding with Aurora A as an Aurora pan-inhibitor.

Based on the results obtained for GSK-1070916, it's evident that the key residues contributing to the ligand selectivity on Aurora B are Arg159 and Asp218. In the Danusertib/Aurora B model, there is no direct interaction between these tertiary amines and Arg159 and Asp218. More significantly, Arg159 and Asp218 instead exhibit an extremely unfavorable interaction with Danusertib.

Therefore, as an Aurora pan-inhibitor, Danusertib provides validation of the Aurora A selectivity mechanism and the Aurora B selectivity mechanism discussed previously.

CHAPTER FIVE

5.1 Conclusion

Aurora kinases, which are potent targets in cancer therapy, exhibit highly conserved homology. They possess only four different residues in the active site: Leu215, Thr217, Val218, and Arg220 in Aurora A, and Arg159, Glu161, Leu162, and Lys164 in Aurora B. This sequence and structural similarity can result in a lack of selectivity and off-target toxicity of kinase inhibitors. Therefore, understanding the selectivity of Aurora kinase inhibitors remains a top priority for designing kinase inhibitors and evaluating clinical safety. Due to the high efficiency and low cost of molecular dynamics simulations, they were employed to study the subtype selectivity mechanism of the inhibitors LY3295668, MK-5108, Alisertib, GSK-1070916, and Danusertib to Aurora A and B. According to the results of these five inhibitors, the binding free energies obtained from the simulations are consistent with the experimentally measured bioactivity data (IC_{50}) that has previously been reported. The key residue responsible for the selectivity of LY3295668, MK-5108 and Alisertib to Aurora A are Thr217 and Arg220/137, while the key functional group in these three Aurora A selective inhibitors is carboxylate group which is confirmed contributes the most significant binding free energy in all Aurora A selective inhibitor with Aurora A models in this study. The key residues responsible for the selectivity of GSK-1070916 to Aurora B are Arg159 and Asp218, while the key functional group in GSK-1070916 is the tertiary amine with methyl group. The results of the Aurora pan-inhibitor Danusertib accord with the selectivity mechanism of Aurora A from LY3295668, MK-5108 and Alisertib and the selectivity mechanism of Aurora B

from GSK-1070916.

Overall, the inhibitor with a carboxylate group is more likely to be an Aurora A selective inhibitor, while the inhibitor with a tertiary amine with methyl group is more likely to be an Aurora B selective inhibitor. The structural information obtained from these studies offers valuable insights into the mechanism of subtype selectivity for Aurora kinase inhibitors, thereby facilitating the further development of highly selective and potent inhibitors as potential drug candidates for cancer therapy.

5.2 Future Work

5.2.1 Selectivity on Aurora B over Aurora C

Although Aurora C primarily acts on germ cells and has minimal involvement with cancer, numerous experiments have indicated that the selectivity profiles of Aurora B and C are highly similar. Therefore, it is imperative to distinguish between Aurora B and Aurora C when Aurora B selective inhibitors bind to Aurora kinases. Obtaining a deeper understanding of the mechanism underlying the high selectivity of Aurora B over C is necessary.

5.2.2 IC_{50} data from biological experiments

Since there is a lack of IC_{50} data in the inhibitor library, it is also necessary to improve the inhibitor library through biological experiments in the future. And we can first perform molecular dynamics simulations on these inhibitors and then use the IC_{50} data obtained from biological experiments to confirm the correctness of the conclusions.

References

1. Friedenreich CM. Physical activity and cancer prevention: from observational to intervention research. *Cancer Epidemiol Biomarkers Prev.* 2001; 10: 287-301.
2. Martel C, Georges D, Bray F, Ferlay J, Clifford GM. Global burden of cancer attributable to infections in 2018: a worldwide incidence analysis. *Lancet Glob Health*. 2020; 8 (2):e180-e190.
3. Fearon K, Strasser F, Anker SD, Bosaeus I, Bruera E, Fainsinger RL, et al. "Definition and classification of cancer cachexia: an international consensus". *The Lancet. Oncology.* 2001; 12 (5): 489–95.
4. Tolar J, Neglia JP. "Transplacental and other routes of cancer transmission between individuals". *Journal of Pediatric Hematology/Oncology.* 2003; 25 (6): 430–4.
5. Brenner DR, Poirier A, Woods RR, Ellison LF, Billette JM, Demers AA, Zhang SX, Yao C, Finley C, Fitzgerald N, Saint-Jacques N, Shack L, Turner D, Holmes E; Canadian Cancer Statistics Advisory Committee. Projected estimates of cancer in Canada in 2022. *CMAJ*. 2022; 194 (17): E601-E607.
6. Manning G, Whyte DB, Martinez R, Hunter T, Sudarsanam S. "The protein kinase complement of the human genome". *Science*. 2002; 298 (5600): 1912–1934.
7. Bolanos-Garcia V M (2005). Aurora kinases. *The International Journal of Biochemistry & Cell Biology*. 37, 1572–1577.
8. Du, R., Huang, C., Liu, K (2021). et al. Targeting AURKA in Cancer: molecular mechanisms and opportunities for Cancer therapy. *Mol Cancer*. 20 (15). https://doi.org/10.1186/s12943-020-01305-3
9. Bolanos-Garcia V M (2005). Aurora kinases. *The International Journal of Biochemistry & Cell Biology,* 37, 1572–1577.
10. Fu, J (2007). "Roles of Aurora Kinases in Mitosis and Tumorigenesis". *Molecular Cancer Research*. 5 (1): 1. doi:10.1158/1541-7786.MCR-06-0208.
11. Du, R., Huang, C., Liu, K (2021). et al. Targeting AURKA in Cancer: molecular mechanisms

and opportunities for Cancer therapy. *Mol Cancer.* 20 (15).

12. Sakai H, Urano T, Ookata K, Kim MH, Hirai Y, Saito M, Nojima Y, Ishikawa F (2002). "MBD3 and HDAC1, two components of the NuRD complex, are localized at Aurora-A-positive centrosomes in M phase". *J. Biol. Chem.* 277 (50): 48714–23. doi:10.1074/jbc.M208461200
13. Shindo M, Nakano H, Kuroyanagi H, Shirasawa T, Mihara M, Gilbert DJ, Jenkins NA, Copeland NG, Yagita H, Okumura K (1998). "cDNA cloning, expression, subcellular localization, and chromosomal assignment of mammalian aurora homologues, aurora-related kinase (ARK) 1 and 2". *Biochem. Biophys. Res. Commun.* 244 (1): 285–92. doi:10.1006/bbrc.1998.8250
14. Kimura M, Kotani S, Hattori T, Sumi N, Yoshioka T, Todokoro K, Okano Y (1997). "Cell cycle-dependent expression and spindle pole localization of a novel human protein kinase, Aik, related to Aurora of Drosophila and yeast Ipl1". *J. Biol. Chem.* 272 (21): 13766–71. doi:10.1074/jbc.272.21.13766
15. Ytana Tanaka M, Ueda A, Kanamori H, Ideguchi H, Yang J, Kitajima S, Ishigatsubo Y (2002). "Cell-cycle-dependent regulation of human aurora A transcription is mediated by periodic repression of E4TF1". *J. Biol. Chem.* 277 (12): 10719–26. doi:10.1074/jbc.M108252200
16. Yan M, Wang C, He B, Yang M, Tong M, Long Z, Liu B, Peng F, Xu L, Zhang Y, Liang D, Lei H, Subrata S, Kelley KW, Lam EW, Jin B, Liu Q (2016). Aurora-A Kinase: a potent oncogene and target for cancer therapy. *Medicinal Research Reviews.* 36:1036–1079 doi:10.1002/med.21399.
17. Yang Y, Shen Y, Li S, Jin N, Liu H, Yao X (2012). Molecular dynamics and free energy studies on Aurora kinase A and its mutant bound with MLN8054: insight into molecular mechanism of subtype selectivity. *Molecular BioSystems.* 8:3049–3060. doi:10.1039/c2mb25217a
18. Gong X (2018). Aurora-A kinase inhibition is synthetic lethal with loss of the RB1 tumor suppressor gene. *Cancer Discov.* 18-0469.

19. Falchook GS, Bastida CC, Kurzrock R (2015). Aurora kinase inhibitors in oncology clinical trials: current state of the progress. *Seminars in Oncology.* 42 (6):832–848. doi:10.1053/j.seminoncol.2015.09.022.
20. Crane R, Gadea B, Littlepage L, Wu H, Ruderman JV (2004). "Aurora A, meiosis and mitosis". *Biol*. Cell. 96 (3): 215–29. doi:10.1016/j.biolcel.2003.09.008
21. Conte N, Delaval B, Ginestier C, Ferrand A, Isnardon D, Larroque C, Prigent C, Séraphin B, Jacquemier J, Birnbaum D (2003). "TACC1-chTOG-Aurora A protein complex in breast cancer". *Oncogene*. 22 (50): 8102–16. doi:10.1038/sj.onc.1206972
22. Gigoux V, L'Hoste S, Raynaud F (2002). "Identification of Aurora kinases as RasGAP Src homology 3 domain-binding proteins". *J. Biol. Chem.* 277 (26): 23742–6. doi:10.1074/jbc.C200121200
23. Sugiyama K, Sugiura K, Hara T (2002). "Aurora-B associated protein phosphatases as negative regulators of kinase activation". *Oncogene.* 21 (20): 3103–11. doi:10.1038/sj.onc.1205432
24. Bischoff, J. R.; Anderson, L; Zhu, Y; Mossie, K; Ng, L; Souza, B; Schryver, B; Flanagan, P; Clairvoyant, F; Ginther, C; Chan, C. S.; Novotny, M; Slamon, D. J.; Plowman, G. D. (1998). "A homologue of Drosophila aurora kinase is oncogenic and amplified in human colorectal cancers". *The EMBO Journal.* 17 (11): 3052–65.
25. Honda, R; Körner, R; Nigg, E. A. (2003). "Exploring the functional interactions between Aurora B, INCENP, and survivin in mitosis". *Molecular Biology of the Cell*. 14 (8): 3325–41. doi:10.1091/mbc.E02-11-0769.
26. Adams, R. R.; Carmena, M; Earnshaw, W. C. (2001). "Chromosomal passengers and the (aurora) ABCs of mitosis". *Trends in Cell Biology.* 11 (2): 49–54. doi:10.1016/s0962-8924 (00)01880-8
27. Murata-Hori, M; Tatsuka, M; Wang, Y. L. (2002). "Probing the dynamics and functions of aurora B kinase in living cells during mitosis and cytokinesis". *Molecular Biology of the Cell.* 13 (4): 1099–108. doi:10.1091/mbc.01-09-0467

28. Delaval B, Ferrand A, Conte N, Larroque C, Hernandez-Verdun D, Prigent C, Birnbaum D (2004). "Aurora B -TACC1 protein complex in cytokinesis". *Oncogene.* 23 (26): 4516–22. doi:10.1038/sj.onc.1207593

29. Gürtler U, Tontsch-Grunt U, Jarvis M, Zahn SK, Boehmelt G, Quant J, Adolf GR, Solca F (2010). "Effect of BI 811283, a novel inhibitor of Aurora B kinase, on tumor senescence and apoptosis". *J. Clin. Oncol*. 28 (15 Suppl e13632): e13632. doi:10.1200/jco.2010.28.15_suppl.e13632

30. Chen J, Jin S, Tahir SK (2003). "Survivin enhances Aurora-B kinase activity and localizes Aurora-B in human cells". *J. Biol. Chem.* 278 (1): 486–90. doi:10.1074/jbc.M211119200.

31. Morrison C, Henzing AJ, Jensen ON (2002). "Proteomic analysis of human metaphase chromosomes reveals topoisomerase II alpha as an Aurora B substrate". *Nucleic Acids Res.* 30 (23): 5318–27. doi:10.1093/nar/gkf665. PMC 137976.

32. Strausberg RL, Feingold EA, Grouse LH (2003). "Generation and initial analysis of more than 15,000 full-length human and mouse cDNA sequences". *Proc. Natl. Acad. Sci. U.S.A.* 99 (26): 16899–903. doi:10.1073/pnas.242603899

33. Zhang Y, Jiang C, Li H, Lv F, Li X, Qian X, Fu L, Xu B, Guo X (2015). Elevated Aurora B expression contributes to chemoresistance and poor prognosis in breast cancer. Int J Clin Exp Pathol. 2015 Jan 1;8 (1):751-7.

34. Bernard M, Sanseau P, Henry C, Couturier A, Prigent C (1998). "Cloning of STK13, a third human protein kinase related to Drosophila aurora and budding yeast Ipl1 that maps on chromosome 19q13.3-ter". *Genomics*. 53 (3): 406–9. doi:10.1006/geno.1998.5522

35. Minoshima Y, Kawashima T, Hirose K (2003). "Phosphorylation by aurora B converts MgcRacGAP to a RhoGAP during cytokinesis". *Dev. Cell.* 4 (4): 549–60. doi:10.1016/S1534-5807 (03)00089-3

36. Prigent C, Gill R, Trower M, Sanseau P (2001). "In silico cloning of a new protein kinase, Aik2, related to Drosophila Aurora using the new tool: EST Blast". *In Silico Biol. (*Gedrukt). 1 (2): 123–8.

37. Khan J, Ezan F, Crémet JY, Fautrel A, Gilot D, Lambert M, Benaud C, Troadec MB, Prigent C (2011). "Overexpression of active Aurora-C kinase results in cell transformation and tumour formation". *PLOS ONE*. 6 (10): e26512. doi:10.1371/journal.pone.0026512

38. Crosio C, Fimia GM, Loury R, Kimura M, Okano Y, Zhou H, Sen S, Allis CD, Sassone-Corsi P (2002). "Mitotic phosphorylation of histone H3: spatio-temporal regulation by mammalian Aurora kinases". *Molecular and Cellular Biology.* 22 (3): 874–85. doi:10.1128/MCB.22.3.874-885.2002.

39. Khan J, Ezan F, Crémet JY, Fautrel A, Gilot D, Lambert M, Benaud C, Troadec MB, Prigent C (2011). "Overexpression of active Aurora-C kinase results in cell transformation and tumour formation". *PLOS ONE.* 6 (10): e26512. doi:10.1371/journal.pone.0026512 A

40. Nna E, Madukwe J, Egbujo E, Obiorah C, Okolie C, Echejoh G, Yahaya A, Adisa J, Uzoma I (2013). "Gene expression of Aurora kinases in prostate cancer and nodular hyperplasia tissues". *Medical Principles and Practice.* 22 (2): 138–43. doi:10.1159/000342679

41. Fujii S, Srivastava V, Hegde A, Kondo Y, Shen L, Hoshino K, Gonzalez Y, Wang J, Sasai K, Ma X, Katayama H, Estecio MR, Hamilton SR, Wistuba I, Issa JP, Sen S (2015). "Regulation of AURKC expression by CpG island methylation in human cancer cells". *Tumour Biology.* 36 (10): 8147–58. doi:10.1007/s13277-015-3553-5

42. Jing, X. L. & Chen, S. W (2021). Aurora kinase inhibitors: a patent review (2014-2020). *Expert Opin. Ther. Pat*. 31, 625–644.

43. Albanese, S. K (2020). Is Structure-Based Drug Design Ready for Selectivity Optimization? *J. Chem. Inf. Model.* 60, 6211–6227.

44. Yang, J (2007). AZD1152, a novel and selective aurora B kinase inhibitor, induces growth arrest, apoptosis, and sensitization for tubulin depolymerizing agent or topoisomerase II inhibitor in human acute leukemia cells in vitro and in vivo. *Blood*. 110, 2034–2040.

45. Damodaran, A. P., Vaufrey, L., Gavard, O. & Prigent, C (2017). Aurora A Kinase Is a Priority Pharmaceutical Target for the Treatment of Cancers. *Trends Pharmacol. Sci*. 38, 687–700.

46. Yan X, Cao L, Li Q, Wu Y, Zhang H, Saiyin H, Liu X, Zhang X, Shi Q, Yu L (2005). "Aurora

C is directly associated with Survivin and required for cytokinesis". *Genes to Cells*. 10 (6): 617–26. doi:10.1111/j.1365-2443.2005.00863.x

47. Cicenas, J (2016). The Aurora kinase inhibitors in cancer research and therapy. *J. Cancer Res. Clin. Oncol.* 142, 1995–2012.
48. Yang, G (2010). Aurora kinase A promotes ovarian tumorigenesis through dysregulation of the cell cycle and suppression of BRCA2. *Clin. Cancer Res.* 16, 3171–3181.
49. Lee, E. C. Y., Frolov, A., Li, R., Ayala, G. & Greenberg, N. M (2006). Targeting aurora kinases for the treatment of prostate cancer. *Cancer Res*. 66, 4996–5002.
50. Pradhan, T., Gupta, O., Singh, G. & Monga, V (2021). Aurora kinase inhibitors as potential anticancer agents: Recent advances. Eur. J. *Med. Chem.* 221, 113495.
51. Karaman, M. W (2008). A quantitative analysis of kinase inhibitor selectivity. *Nat. Biotechnol.* 26, 127–132.
52. Davis, M. I (2011). Comprehensive analysis of kinase inhibitor selectivity. *Nat. Biotechnol.* 29, 1046–1051.
53. Keen, N. Taylor, S (2004). Aurora-kinase inhibitors as anticancer agents. *Nat. Rev. Cancer*. 4, 927–936.
54. Zhang Z, Xu Y, Wu J, Shen Y, Cheng H, Xiang Y (2019). Exploration of the selective binding mechanism of protein kinase Aurora A selectivity via a comprehensive molecular modeling study. *PeerJ,* 7:e7832
55. Zhao D, Kovacs AH, Campbell M, Floriano W, Hou J (2022). Exploring the structural basis of a subtype selective inhibitor for Aurora kinase B over Aurora kinase A by molecular dynamics simulations. *Research Square*. doi: 10.21203/rs.3.rs-1942448/v1.
56. Nair JS, Ho AL, Schwartz GK (2012). The induction of polyploidy or apoptosis by the Aurora A kinase inhibitor MK8745 is p53-dependent. *Cell Cycle*. 15;11 (4):807-17. doi: 10.4161/cc.11.4.19323. Epub 2012 Feb 15. PMID: 22293494; PMCID: PMC3318110.
57. Shimomura T, Hasako S, Nakatsuru Y, Mita T, Ichikawa K, Kodera T, Sakai T, Nambu T, Miyamoto M, Takahashi I, Miki S, Kawanishi N, Ohkubo M, Kotani H, Iwasawa Y (2010).

MK-5108, a highly selective Aurora-A kinase inhibitor, shows antitumor activity alone and in combination with docetaxel. *Mol Cancer Ther.* 9 (1):157-66. doi: 10.1158/1535-7163.MCT-09-0609. Epub 2010 Jan 6. PMID: 20053775.

58. Gong X, Du J, Parsons SH, Merzoug FF, Webster Y (2019). Aurora A Kinase Inhibition Is Synthetic Lethal with Loss of the RB1 Tumor Suppressor Gene. *Cancer Discov.* 9 (2):248-263. doi: 10.1158/2159-8290.CD-18-0469. Epub 2018 Oct 29. PMID: 30373917.
59. Sootome H, Miura A, Masuko N, Suzuki T, Uto Y, Hirai H (2020). Aurora A Inhibitor TAS-119 Enhances Antitumor Efficacy of Taxanes In Vitro and In Vivo: Preclinical Studies as Guidance for Clinical Development and Trial Design. *Mol Cancer Ther.* 19 (10):1981-1991. doi: 10.1158/1535-7163.MCT-20-0036. Epub 2020 Aug 11. PMID: 32788206.
60. Bavetsias V, Linardopoulos S (2015). Aurora Kinase Inhibitors: Current Status and Outlook. *Front Oncol.* 5:278. doi: 10.3389/fonc.2015.00278. PMID: 26734566; PMCID: PMC4685048.
61. Manfredi MG, Ecsedy JA, Meetze KA, Balani SK, Burenkova O (2007). Antitumor activity of MLN8054, an orally active small-molecule inhibitor of Aurora A kinase. *Proc Natl Acad Sci U S A.* 104 (10):4106-11. doi: 10.1073/pnas.0608798104. Epub 2007 Feb 23. PMID: 17360485; PMCID: PMC1820716.
62. Wang LX, Wang JD, Chen JJ, Long B, Liu LL (2016). Aurora A Kinase Inhibitor AKI603 Induces Cellular Senescence in Chronic Myeloid Leukemia Cells Harboring T315I Mutation. *Sci Rep*. 6:35533. doi: 10.1038/srep35533. PMID: 27824120; PMCID: PMC5099696.
63. Lakkaniga NR, Zhang L, Belachew B, Gunaganti N, Frett B, Li HY (2020). Discovery of SP-96, the first non-ATP-competitive Aurora Kinase B inhibitor, for reduced myelosuppression. *Eur J Med Chem*. 203:112589. doi: 10.1016/j.ejmech.2020.112589. PMID: 32717530.
64. Yang J, Ikezoe T, Nishioka C, Tasaka T, Taniguchi A (2007). AZD1152, a novel and selective aurora B kinase inhibitor, induces growth arrest, apoptosis, and sensitization for tubulin depolymerizing agent or topoisomerase II inhibitor in human acute leukemia cells in vitro

and in vivo. *Blood.* 110 (6):2034-40. doi: 10.1182/blood-2007-02-073700. PMID: 17495131.

65. Jetton N, Rothberg KG, Hubbard JG, Wise J, Li Y, Ball HL, Ruben L (2009). The cell cycle as a therapeutic target against Trypanosoma brucei: Hesperadin inhibits Aurora kinase-1 and blocks mitotic progression in bloodstream forms. *Mol Microbiol.* 72 (2):442-58. doi: 10.1111/j.1365-2958.2009.06657.x. PMID: 19320832; PMCID: PMC2697958.
66. Adams ND, Adams JL, Burgess JL, Chaudhari AM, Copeland RA (2010).Discovery of GSK1070916, a potent and selective inhibitor of Aurora B/C kinase. *J Med Chem.* 53 (10):3973-4001. doi: 10.1021/jm901870q. PMID: 20420387.
67. Zi D, Zhou ZW, Yang YJ, Huang L, Zhou ZL, He SM, He ZX, Zhou SF (2015). Danusertib Induces Apoptosis, Cell Cycle Arrest, and Autophagy but Inhibits Epithelial to Mesenchymal Transition Involving PI3K/Akt/mTOR Signaling Pathway in Human Ovarian Cancer Cells. *Int J Mol Sci.* 16 (11):27228-51. doi: 10.3390/ijms161126018. PMID: 26580601; PMCID: PMC4661876.
68. Sini P, Gürtler U, Zahn SK, Baumann C, Rudolph D (2016). Pharmacological Profile of BI 847325, an Orally Bioavailable, ATP-Competitive Inhibitor of MEK and Aurora Kinases. *Mol Cancer Ther*. 2388-2398. doi: 10.1158/1535-7163.MCT-16-0066. Epub 2016 Aug 5. PMID: 27496137.
69. Choudhury C, Priyakumar UD, Sastry GN (2015). "Dynamics based pharmacophore models for screening potential inhibitors of mycobacterial cyclopropane synthase". *Journal of Chemical Information and Modeling.* 55 (4): 848‑60. doi:10.1021/ci500737b. PMID 25751016.
70. Kitchen DB, Decornez H, Furr JR, Bajorath J (2004). "Docking and scoring in virtual screening for drug discovery: methods and applications". Nature Reviews. *Drug Discovery.* 3 (11): 935‑49. doi:10.1038/nrd1549. PMID 15520816. S2CID 1069493
71. J. Eberhardt, D. Santos-Martins, A. F. Tillack, and S. Forli. (2021). AutoDock Vina 1.2.0: New Docking Methods, Expanded Force Field, and Python Bindings. *Journal of Chemical Information and Modeling.*

72. O. Trott, A. J. Olson, AutoDock Vina: improving the speed and accuracy of docking with a new scoring function, efficient optimization and multithreading, *Journal of Computational Chemistry.* 31 (2010) 455-461

73. Hatmal MM, Jaber S, Taha MO (2016). "Combining molecular dynamics simulation and ligand-receptor contacts analysis as a new approach for pharmacophore modeling: beta-secretase 1 and check point kinase 1 as case studies". *Journal of Computer-aided Molecular Design*. 30 (12): 1149 – 1163. Bibcode:2016JCAMD..30.1149H. doi:10.1007/s10822-016-9984-2. PMID 27722817. S2CID 11561853

74. Case DA, Cheatham TE 3rd, Darden T, Gohlke H, Luo R, Merz KM Jr, Onufriev A (2005). The Amber biomolecular simulation programs. *J Comput Chem*. 26 (16):1668-88. doi: 10.1002/jcc.20290. PMID: 16200636; PMCID: PMC1989667.

75. Case D. A.; Darden T. A.; Cheatham T. E.; Simmerling C. L.; Wang J.; Duke R. E.; Luo R. C. W.; Zhang W.; Merz K. M.; Roberts B.; Hayik S.; Roitberg A.; Seabra G.; Swails J.; Kolossváry I.; Wong K. F.; Paesani F.; Vanicek J.; Wolf R. M.; Liu J.; Wu X.; Steinbrecher T.; Gohlke H.; Cai Q.; Ye X.; Wang J.; Hsieh M.-J.; Cui D. R. R.; Mathews D. H.; Seetin M. G.; Salomon-Ferrer R.; Sagui C.; Babin V.; Luchko S. G.; Kovalenko A.; Kollman P. A. (2020). Amber 2020. University of California,San Francisco. https://ambermd.org.

76. Genheden S, Ryde U (2015). The MM/PBSA and MM/GBSA methods to estimate ligand-binding affinities. *Expert Opin Drug Discov.* 10 (5):449-61. doi: 10.1517/17460441.2015.1032936. Epub 2015 Apr 2. PMID: 25835573; PMCID: PMC4487606.

77. Tuccinardi, T. (2021). What is the current value of MM/PBSA and MM/GBSA methods in drug discovery? *Expert Opinion on Drug Discovery,* 16 (11), 1233 – 1237. https://doi.org/10.1080/17460441.2021.1942836

78. H.M. Berman, J. Westbrook, Z. Feng, G. Gilliland, T.N. Bhat, H. Weissig, I.N. Shindyalov, P.E. Bourne (2000). The Protein Data Bank. *Nucleic Acids Research*, 28: 235-242. https://doi.org/10.1093/nar/28.1.235

79. Jumper, J et al (2021). Highly accurate protein structure prediction with AlphaFold. *Nature*.
80. Varadi, M et al (2024). AlphaFold Protein Structure Database in 2024: providing structure coverage for over 214 million protein sequences. *Nucleic Acids Research*.
81. Strzyz, P (2023). Lasker Award for AlphaFold. *Nat Rev Mol Cell Biol*. 24, 774 https://doi.org/10.1038/s41580-023-00671-2
82. Willems E, Dedobbeleer M, Digregorio M, Lombard A, Lumapat PN, Rogister B (2018). The functional diversity of Aurora kinases: a comprehensive review. *Cell Div.* 13:1–3. doi:10.1186/s13008-018-0040-6.
83. Elkins, J. M., Santaguida, S., Musacchio, A. & Knapp, S (2012). Crystal structure of human aurora B in complex with INCENP and VX-680. *J. Med. Chem.* 55, 7841–7848.
84. Lin, Z. Z (2010). Significance of Aurora B overexpression in hepatocellular carcinoma. Aurora B Overexpression in HCC. *BMC Cancer* .10.
85. Schwartz, G. K (2013). Phase I study of Barasertib (AZD1152), a selective inhibitor of Aurora B kinase, in patients with advanced solid tumors. *Invest. New Drugs.* 31, 370–380.
86. Carvajal, R. D.; Tse, A.; Schwartz, G. K. (2006). "Aurora Kinases: New Targets for Cancer Therapy". *Clinical Cancer Research.* 12 (23): 6869–6875. doi:10.1158/1078-0432.CCR-06-1405
87. Yang, Y (2012). Molecular dynamics and free energy studies on Aurora kinase A and its mutant bound with MLN8054: Insight into molecular mechanism of subtype selectivity. *Mol. Biosyst*. 8, 3049–3060.
88. Lengauer T, Rarey M (1996). "Computational methods for biomolecular docking". *Current Opinion in Structural Biology.* 6 (3): 402–6. doi:10.1016/S0959-440X (96)80061-3
89. Kirkpatrick, P (2004). Gliding to success. *Nat Rev Drug Discov* 3, 299. https://doi.org/10.1038/nrd1364
90. Mostashari-Rad T, Arian R, Mehridehnavi A, Fassihi A, Ghasemi F (2019). "Study of CXCR4 chemokine receptor inhibitors using QSPR andmolecular docking methodologies". *Journal of Theoretical and Computational Chemistry.* 178 (4).

doi:10.1142/S0219633619500184

91. M. Augusto, S. Sallem, S. A. de Sousa and F. J. da Silva e Silva (2007). AutoGrid: Towards an Autonomic Grid Middleware. *16th IEEE International Workshops on Enabling Technologies: Infrastructure for Collaborative Enterprises*. 223-228. doi: 10.1109/WETICE.2007.4407158.
92. J.A.T. Ewing, I.D. Kuntz (1997). Critical evaluation of search algorithms for automated molecular docking and database screening. *J Comput Chem,* 18, p. 1175
93. Wei BQ, Weaver LH, Ferrari AM, Matthews BW, Shoichet BK (2004). "Testing a flexible-receptor docking algorithm in a model binding site". *Journal of Molecular Biology*. 337 (5): 1161–82. doi:10.1016/j.jmb.2004.02.015
94. Arcon JP, Turjanski AG, Martí MA, Forli S (2021). Biased Docking for Protein-Ligand Pose Prediction. *Methods in Molecular Biology.* Vol. 2266. New York, NY: Springer US. pp. 39–72. doi:10.1007/978-1-0716-1209-5_3
95. Roy K, Kar S, Das RN (2015). Other Related Techniques. *Understanding the Basics of QSAR for Applications in Pharmaceutical Sciences and Risk Assessment*. 357–425. doi: 10.1016/B978-0-12-801505-6.00010-7.
96. Wang, J., Wolf, R. M.; Caldwell, J. W.;Kollman, P. A.; Case, D. A (2004). "Development and testing of a general AMBER force field". *Journal of Computational Chemistry*. 25, 1157-1174
97. O. Trott, A. J. Olson (2010). AutoDock Vina: improving the speed and accuracy of docking with a new scoring function, efficient optimization and multithreading. *Journal of Computational Chemistry*. 31,455-461
98. Stephan S, Thol M, Vrabec J, Hasse H (2019). "Thermophysical Properties of the Lennard-Jones Fluid: Database and Data Assessment". *Journal of Chemical Information and Modeling.* 59 (10): 4248–4265. doi:10.1021/acs.jcim.9b00620
99. Schlick T (1996). "Pursuing Laplace's Vision on Modern Computers". Mathematical Approaches to Biomolecular Structure and Dynamics. *The IMA Volumes in Mathematics and*

its Applications. Vol. 82. pp. 219–247. doi:10.1007/978-1-4612-4066-2_13

100. Stephan S, Horsch MT, Vrabec J, Hasse H (2019). "MolMod – an open access database of force fields for molecular simulations of fluids". *Molecular Simulation.* 45 (10): 806–814. doi:10.1080/08927022.2019.1601191

101. Raval A, Piana S, Eastwood MP, Dror RO, Shaw DE (2012). "Refinement of protein structure homology models via long, all-atom molecular dynamics simulations". *Proteins.* 80 (8): 2071–2079. doi:10.1002/prot.24098

102. Ryckaert, J. P., Ciccotti, G. & Berendsen, H. J. C (1977). Numerical integration of the cartesian equations of motion of a system with constraints: molecular dynamics of n-alkanes. *J. Comput. Phys*. 23, 327–341.

103. Darden, T., York, D. & Pedersen, L (1993). Particle mesh Ewald: An N·log (N) method for Ewald sums in large systems. *J. Chem. Phys.* 98, 10089–10092.

104. Damm KL, Carlson HA (2006). "Gaussian-Weighted RMSD Superposition of Proteins: A Structural Comparison for Flexible Proteins and Predicted Protein Structures". *Biophys J.* 90 (12): 4558–4573. Bibcode:2006BpJ....90.4558D. doi:10.1529/biophysj.105.066654

105. Ying Y, Yulin S, Shuyan L, Nengzhi J, Huanxiang L, Xiaojun Y (2012). Molecular dynamics and free energy studies on Aurora kinase A and its mutant bound with MLN8054: insight into molecular mechanism of subtype selectivity. *Mol. BioSyst.* 8, 3049-3060

106. Hou T, Wang J, Li Y, Wang W (2011). Assessing the performance of the MM/PBSA and MM/GBSA methods. 1. The accuracy of binding free energy calculations based on molecular dynamics simulations. *J Chem Inf Model*. 51 (1):69-82. doi: 10.1021/ci100275a.

107. Maghsoud Y, Dong C, Cisneros GA (2023). Investigation of the Inhibition Mechanism of Xanthine Oxidoreductase by Oxipurinol: A Computational Study. *J Chem Inf Model.* 63 (13):4190-4206. doi: 10.1021/acs.jcim.3c00624.

108. Genheden S, Ryde U (2015). The MM/PBSA and MM/GBSA methods to estimate ligand-binding affinities. *Expert Opin Drug Discov.* 10 (5):449-61. doi: 10.1517/17460441.2015.1032936.

109. Jiao D, Zhang J, Duke RE (2009). Trypsin–ligand binding free energies from explicit and implicit solvent simulations with polarizable potential. *J Comput Chem*. 30:1701–11.

110. Kongsted J, Ryde U (2009). An improved method to predict the entropy term with the MM/PBSA approach. *J Comput-Aided Mol Design*. 23:63–71.

111. Miller, B. R (2012). MMPBSA.py: An efficient program for end-state free energy calculations. J. Chem. Theory Comput. 8, 3314–3321.

112. Gohlke H, Kiel C (2003). Insights into protein-protein binding by binding free energy calculation and free energy decomposition for the Ras-Raf and Ras-RalGDS complexes. *J Mol Biol.* 330 (4):891-913. doi: 10.1016/s0022-2836 (03)00610-7.

113. Wang J, Hou T, Xu X (2006). Recent Advances in Free Energy Calculations with a Combination of Molecular Mechanics and Continuum Models. *Current Computer-Aided Drug Design.* 2 (3) . doi: https://dx.doi.org/10.2174/157340906778226454